

NUCLEAR STRUCTURE -- EXPERIMENT

M. Samuel, B.A. Brown, D. Mikolas, J. Nolen, B. Sherrill, J. Stevenson,
J. Winfield and Z. Q. Xie

The MSU Reaction Products Mass Separator was used to measure the beta decay half-lives of seven neutron rich fragments produced by the fragmentation of a $E/A=35$ MeV ^{22}Ne beam. The first measurement of the half-life of ^{17}B was made along with measurements of the half-lives of ^{19}N , ^{17}C , ^{15}B , ^{13}B , ^{12}B , and ^9Li . ^{19}C was also observed, but not in sufficient quantities to make a half-life measurement.

Copper, tin, and tantalum targets were tested during trials that led to significant improvements in yields, transport, and resolution. The beam intensity reached 0.5 μA on target, melting both the tin and copper targets and causing the tantalum target to glow visibly. The final data was taken using a stopping tantalum target.

The focal plane detector was a two element Si ΔE , E telescope with thicknesses of 100 μm and 1 mm respectively. Aluminum degraders were used in front of the telescope so that isotopes of interest were stopped in the Si E detector. In order to minimize dead time, another 100 μm thick Si detector was placed behind the telescope and used to veto He and Li isotopes that punched through the E detector. These isotopes had count rates that were much higher than those of the isotopes of interest.

When an ion was implanted, the beam was turned off in approximately 40 μs by switching the rf phase on one of the dees of the K500 cyclotron, and remained off for a preset time equal to several half-lives of the longest lived isotope of interest present at the focal plane. During the beam-off period, all counts in the E detector above a threshold of approximately 0.5 MeV were recorded.

The analysis of the data for the cases of ^{12}B , ^{13}B , ^{15}B , and ^{17}B was complicated by a strong short lived background attributed to

(n,γ) reactions induced by thermal neutrons in the vault. In addition, the background also contained a large constant component due to long lived isotopes implanted in the silicon and long lived daughters, as well as cosmic rays and activity elsewhere in the vault. The background was conveniently parameterized as an exponential plus a constant using data from long lived or stable isotopes. For the longer lived isotopes ^9Li , ^{17}C , and ^{19}N , the effect of the short-lived component of the background was eliminated by discarding the first 31.2 ms of the beam-off period. Thus, only the constant component of the background had to be considered.

The beta decay time spectra were fit with a newly developed code using the method of maximum likelihood for Poisson statistics.^{1,2} The maximum likelihood technique was used instead of the χ^2 method because of the low statistics data. The function used to fit each decay spectrum consisted of an exponential plus the appropriate background parameterization normalized to the number of incident ions for the spectrum. The results of these fits are shown in Table 1.

The theoretical predictions shown in Table 1 are the results of shell-model calculations carried out in the spsd model space in which the $0s_{1/2}$, $0p_{3/2}$, $0p_{1/2}$, $1s_{1/2}$, and $0d_{5/2}$ orbitals are active. The residual-interaction matrix elements connecting the Op-shell orbitals were taken from the results of a fit to Op-shell energy levels in the $A = 10-15$ mass region obtained by Millener.¹⁰ The matrix elements connecting the 1s0d-shell orbitals were taken from the fit to 1s0d-shell energy levels in the $A = 18-38$ mass region obtained by Wildenthal.¹¹ All other matrix elements, including the cross-shell matrix elements connecting the $0s$, $0p$, and $1s0d$ orbitals were calculated with the residual

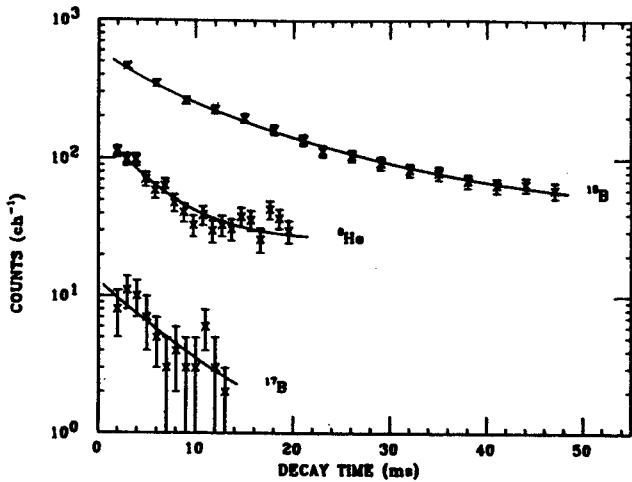
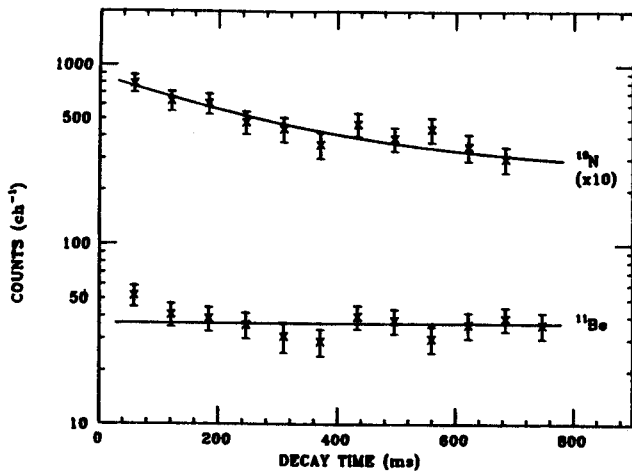


Fig. 1. Beta decay half-life data. Curves shown are fits to an exponential plus an appropriate background as explained in the text. The uncorrected spectra obtained from the incident ions ${}^6\text{He}$ and ${}^{11}\text{Be}$ are shown as examples of the short-lived and constant components of the background. Both ${}^6\text{He}$ and ${}^{11}\text{Be}$ are long-lived relative to the respective beam-off periods used during data acquisition.

interaction of Millener and Kurath.¹² Within this model space we made a " $0\Omega\omega$ " truncation for the initial state and allowed " $0\Omega\omega$ " and " $1\Omega\omega$ " for the final states. The calculated half-lives include a quenching factor of 0.6 in the $B(GT)$ value. These calculations are based on the experimental Q value for the lowest final state and theoretical excitation energies for the final states.

Table 1

isotope	this measurement	previous measurements	prediction
${}^{19}\text{N}$	$205.0 \pm 62.0 \text{ms}$	$320.0 \pm 100.0 \text{ms}^a$ $210.0^{+200.0}_{-100.0} \text{ms}^b$	620ms
${}^{17}\text{C}$	$161.0 \pm 48.0 \text{ms}$	$202.0 \pm 17.0 \text{ms}^c$ $220.0 \pm 80.0 \text{ms}^a$	
${}^{17}\text{B}$	$5.5 \pm 1.9 \text{ms}$		8.6ms
${}^{15}\text{B}$	$11.0 \pm 2.8 \text{ms}$	$8.8 \pm 0.6 \text{ms}^c$ $11.0 \pm 1.0 \text{ms}^d$ $10.3 \pm 0.4 \text{ms}^b$	9.1ms
${}^{13}\text{B}$	$19.0 \pm 6.0 \text{ms}$	$17.37 \pm 0.16 \text{ms}^e$	19.0ms
${}^{12}\text{B}$	$25.0 \pm 8.0 \text{ms}$	$20.20 \pm 0.02 \text{ms}^f$	22.6ms
${}^9\text{Li}$	$142.0 \pm 43.0 \text{ms}$	$178.3 \pm 4.0 \text{ms}^g$	127.0ms

Beta decay half-lives from this experiment compared to previous experimental results and shell-model predictions.

- a) Ref. 3 d) Ref. 6 f) Ref. 8
 b) Ref. 4 e) Ref. 7 g) Ref. 9
 c) Ref. 5

References

1. T. Aways, NIM 165 317 (1979).
2. T. Aways, NIM 174 237 (1980).
3. J.P. Dufour, R. Del Moral, A. Fleury, F. Hubert, D. Jean, M.S. Pravikoff, H. Delagrande, H. Geissel and K.H. Schmidt, Z. Phys. A324 487 (1986).
4. A.C. Mueller, to be published in Proceedings of the XXV International Winter Meeting on Nuclear Physics, Bormio, Italy, 1987.
5. M.S. Curtin, L.H. Harwood, J.A. Nolen, B. Sherrill, Z.Q. Xie and B.A. Brown, Phys. Rev. Lett. 56 34 (1986).
6. J.P. Dufour, S. Beraud-Sudreau, R. Del Moral, H. Emmermann, A. Fleury, F. Hubert, C. Pointot, M. Pravikoff, J. Frehout, M. Beau, A. Bertin, G. Giraudet, A. Huck, G. Klotz, C. Miede, C. Richard-Serre and H. Delagrange, Z. Phys. A319 237 (1984).
7. F. Ajzenberg-Selove, Nuc. Phys. A449 1 (1986)
8. D.E. Alburger and A.M. Nathan, Phys. Rev. C17 280 (1978)
9. D.E. Alburger and D.H. Wilkinson, Phys. Rev. C13 835 (1976).
10. D.J. Millener, private communication.
11. B.H. Wildenthal, Progress in Particle and Nuclear Physics (Pergamon, New York, 1983), Vol. 11, p. 5.
12. D.J. Millener and D. Kurath, Nucl. Phys. A255, 315 (1975).

J. Stevenson, Y. Chen, J. Nolen, J. Winfield, E. Kashy, W. Benenson,
D. Mikolas, M. Samuel, A.R. Lampis

The possibility that ^{10}He , a highly neutron-rich doubly magic nucleus, may be bound against decay by particle emission has generated both theoretical and experimental investigations.

We report here a search for ^{10}He among projectile-like fragments using a $E/A=30$ MeV ^{18}O beam. A 140 mg/cm^2 tin target was used, which was sufficiently thick to stop the beam and allow study of projectile fragments at zero degrees. The Reaction Product Mass Separator (RPMS) was used to filter the various reaction products emerging at zero degrees. The RPMS consists of a velocity filter (ExB), followed by a dipole magnet. The RPMS focuses in position and momentum and disperses in the mass-to-charge ratio (M/Q). The detector consisted of position sensitive gas counter followed by a silicon telescope consisting of four 1 mm thick lithium drifted silicon detectors. Particles were identified by the energy losses in each element of the telescope and by their M/Q values given by their position at the focal plane. The RPMS was set for a variety of M/Q values, and yields obtained for ^2H , ^3H , ^4He , ^6He , ^8He , ^7Li , ^8Li , ^9Li , and ^{11}Li in addition to the search for ^{10}He .

In the analysis of the data a silicon detector particle identification parameter (PID) was defined $\text{PID}=(E+\Delta E)^\alpha - E^\alpha$ with $\alpha=1.76$. Since the silicon telescope consisted of a stack of four detectors multiple particle identification parameters can be defined. PID1 was defined using the first silicon detector as the ΔE and the sum of the remainder as the E. PID2 was then defined with the second detector as the ΔE . In order for an event to be included, the two particle identification parameters PID1 and PID2 had to agree and the particle had to be near the M/Q=5 line in the focal plane gas counter. The

M/Q=5 line was determined by using the M/Q=4 line and scaling the RPMS magnet settings such that the M/Q=5 line should be in the same location. This procedure was found to work well in going from M/Q=3 to M/Q=4.

Figure 1 shows the events that were seen during a long run at the M/Q=5 setting. The particle identification parameter is an average of PID1 and PID2. The isotopes ^4He , ^6He , and ^8He which are clearly seen are however greatly suppressed since the RPMS is focused for M/Q=5. There are however no counts which appear close to the ^{10}He location.

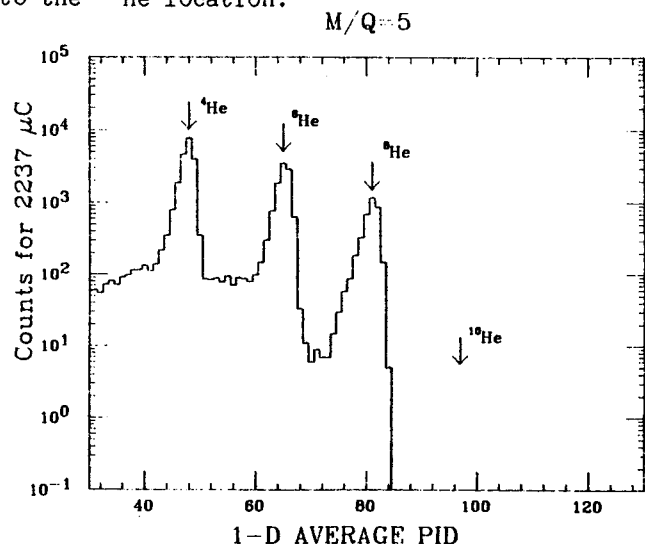


Fig. 1. Helium isotopes observed with the RPMS set for M/Q=5 fragments. No ^{10}He isotopes are observed. The lighter helium isotopes appear but are greatly suppressed at the M/Q=5 mass focus.

The yields of a variety of neutron rich hydrogen, helium, and lithium isotopes were measured. The yields are shown in figure 2 plotted versus the neutron excess $N-Z$. The limit on the yield of ^{10}He based on zero counts is also shown. The rarest observed isotope ^{11}Li is about four orders of magnitude more abundant. An extrapolation of the yield trends in the observed isotopes indicates that we should have observed about 1000 ^{10}He if it were stable.

Production limit of ^{10}He

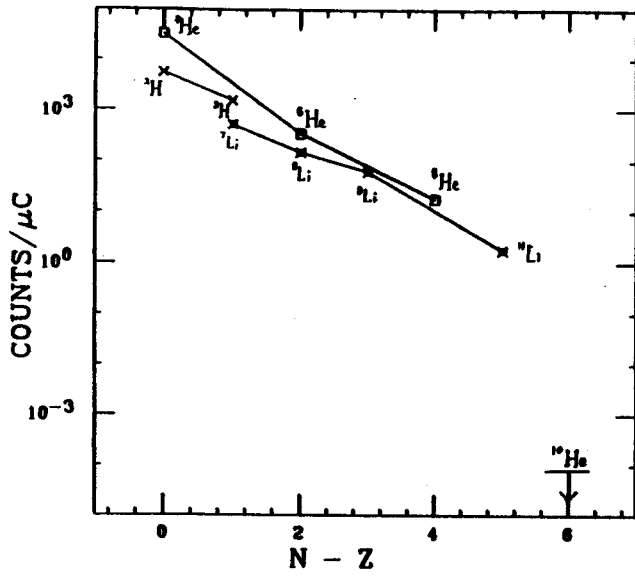


Fig. 2. Plot of the yield of light neutron rich hydrogen, helium and lithium isotopes. The ^{10}He yield is an upper limit based on no counts.

J.S. Winfield, S.M. Austin, Z. Chen, G.M. Crawley, C. Djalali,
K. Dutch, R.J. Smith and M. Torres

At bombarding energies near or above the Fermi energy, nucleon transfer between low-lying discrete states is determined mainly by recoil effects, i.e. the reaction dynamics.¹ At such energies, mass transfer is associated with large momentum transfer, and only the high momentum tails of the incoming and outgoing wave function are important. This results in a roughly exponential decrease of the transfer cross section with increasing bombarding energy (Fig. 1). Such behavior has already been noted in a survey² of light-ion reactions on ^{208}Pb .

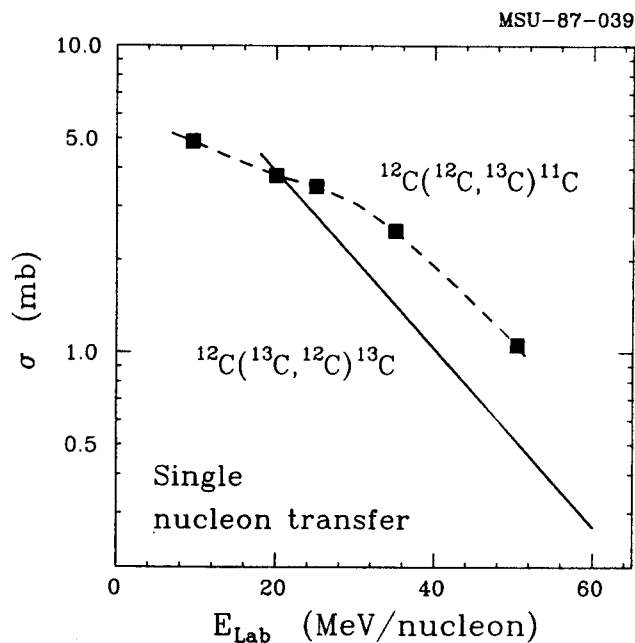


Fig. 1. Dependence of single neutron transfer cross sections on incident energy. The line shows the trend of DWBA predictions for $^{12}\text{C}(^{13}\text{C}, ^{12}\text{C})^{13}\text{C}$ (g.s.) taken from Refs. 1 and 3. The points are experimental results for $^{12}\text{C}(^{12}\text{C}, ^{13}\text{C})^{11}\text{C}$ (g.s.) described in the text. The dashed line is to guide the eye.

One implication of the rapid fall-off of the transfer probability is that at sufficiently high energies, heavy-ion charge exchange reactions will have a negligible contribution from the sequential transfer process compared to the one-step (π -exchange) mechanism of spectroscopic

interest. In the case of the $(^{12}\text{C}, ^{12}\text{N})$ charge exchange reaction, we have shown³ that the critical energy is about 60 MeV/nucleon, based on transfer cross sections calculated with the DWBA and a charge exchange cross section measured at 35 MeV/nucleon.

In one of the few such heavy-ion experiments in the Fermi energy domain, Berthier et al.⁴ studied one nucleon transfer reactions induced by a 50 MeV/nucleon ^{16}O beam on a ^{208}Pb target. Distorted wave Born approximation (DWBA) calculations, which have agreed reasonably well with data at lower bombarding energies, over-predicted their 50 MeV/nucleon data by an order of magnitude. Thus it is important to verify empirically the energy dependence of $^{12}\text{C} + ^{12}\text{C}$ induced transfer reactions rather than rely on DWBA predictions, as was done in Ref. 3.

We have measured the neutron-transfer reaction $^{12}\text{C}(^{12}\text{C}, ^{13}\text{C})^{11}\text{C}$ with beam energies of 25, 35 and 50 MeV/nucleon from the K500 cyclotron at NSCL. The ^{13}C particles were analyzed by the S-320 spectrograph with a resolution of about $E/\Delta E=600$. At 25 and 35 MeV/nucleon, a few spectra for the $(^{12}\text{C}, ^{11}\text{B})$ and $(^{12}\text{C}, ^{10}\text{B})$ reactions also were recorded.

All the spectra show the strong selectivity of heavy-ion transfer reactions at these high bombarding energies: typically only one strong peak is observed (Fig. 2) and this generally consists of relatively high spin states, reflecting the large angular momentum transfer favored by the dynamics. For example, in the $^{12}\text{C}(^{12}\text{C}, ^{13}\text{C})^{11}\text{C}$ spectrum, the strongest peak observed corresponds to the unresolved $3/2^-$, (3.68 MeV) $5/2^+$, (3.85 MeV) states in ^{13}C , and the $5/2^-$, (4.32 MeV) state in ^{11}C . The ground state peak is about eight times weaker than this.

Table 1. Optical parameters used in the DWBA calculations. The column headed "E/A" gives the energy/nucleon for which the parameter set was employed.

V	r	a	W	r _w	a _w	E/A	Ref.
250	0.814	0.626	231.9	0.789	0.60	50	a
180	0.69	0.79	56.7	0.89	0.73	35	b
180	0.735	0.408	600	0.408	0.85	25	c
44	1.05	0.683	28.3	1.05	0.683	10	d

- a) C.-C. Sahm et al., Phys. Rev. C 34,2165(1986).
 b) M. Buenerd et al., Nucl. Phys. A424,313(1984).
 c) H.G. Bohlen et al., Z. Phys. A 308,121(1982).
 d) C.B. Fulmer et al., Phys. Rev. C. 20,670(1979).

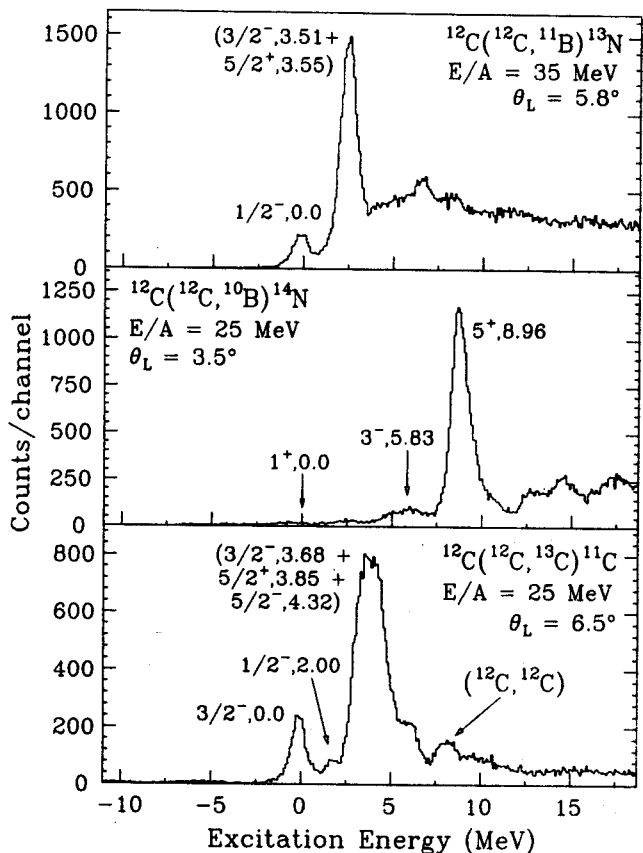


Fig. 2. Spectra of various transfer reactions induced by $^{12}\text{C} + ^{12}\text{C}$ at 25 and 35 MeV/nucleon.

Angular distributions for the $^{12}\text{C}(^{12}\text{C}, ^{13}\text{C})^{11}\text{C}$ reaction leading to the ground states of ^{13}C and ^{11}C are shown in Fig. 3 together with finite-range DWBA predictions. The DWBA calculations were made with the code SATURN-MARS (Ref. 5) and are normalized to the data to fix the spectroscopic factors. The optical model parameters (OMP) used in the calculations are listed in Table 1.

The indistinguishability of the particles in the entrance channel is accounted for by multiplying σ_{tot} , which is integrated out to say 30° , by two. Also given in Table 2 are the measured ⁶ cross section of 3.8 mb at 20 MeV/nucleon and a value of 4.9 mb extracted from the 10 MeV/nucleon data of Ref. 7. The empirical cross sections are plotted as points in Fig. 1. Above about 30 MeV/nucleon, the cross section decreases with approximately the same exponential slope as that predicted for $^{12}\text{C}(^{13}\text{C}, ^{12}\text{C})^{13}\text{C}$. Below about 30 MeV/nucleon,

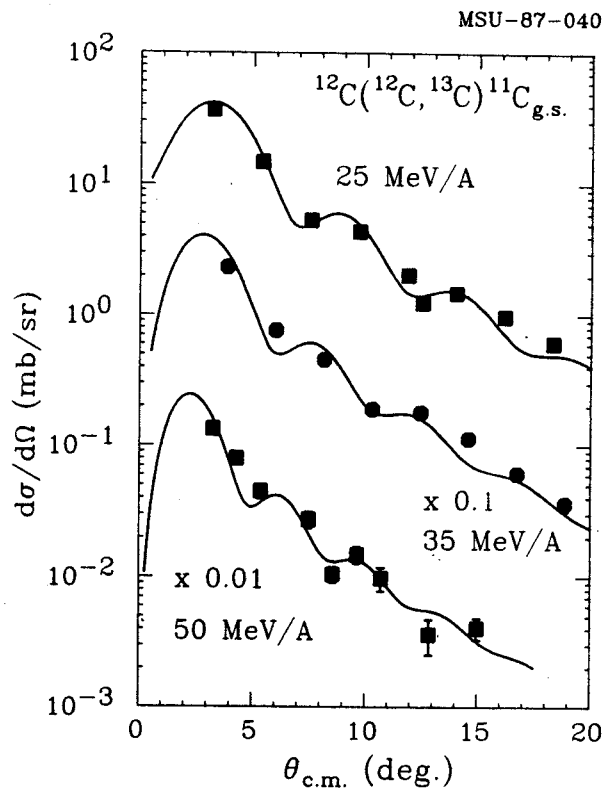


Fig. 3. Angular distributions for $^{12}\text{C}(^{12}\text{C}, ^{13}\text{C})^{11}\text{C}$ (g.s.) at incident energies of 25, 35 and 50 MeV/nucleon. The curves are DWBA calculations described in the text.

In Table 2, the extracted products of the spectroscopic factors are given together with the angle-integrated DWBA cross sections.

Table 2. Products of target and projectile spectroscopic factors and angle-integrated cross sections for the reaction $^{12}\text{C}(^{12}\text{C}, ^{13}\text{C})^{11}\text{C}$.

E/A [MeV]	$C_1^2 S_1 \times C_2^2 S_2$	σ_{tot} [mb]	Ref.
50	3.0	1.06	a
35	1.9	2.5	a
25	2.2	3.5	a
20	1.8	3.8	6
10	2.1	4.9	7

a) present work

the cross section rises less steeply. These features are reproduced by the DWBA calculations, as seen by the approximately constant spectroscopic factors. Calculations with alternative OMPs, when normalized to the data, gave spectroscopic factors within 50% of the values quoted in Table 2. The overall slope of the angular distribution at 50 MeV/nucleon showed a slight dependence on the choice of OMP; the potential indicated in Table 1 gave the best fit (shown in Fig. 3).

1. W. von Oertzen, in Frontiers of Nuclear Dynamics, edited by R.A. Broglia and C.H. Dasso (Plenum, New York, 1985); Phys. Lett. 151B,95(1985).
2. T. Kurihara and M. Sakai, Phys. Lett. 133B, 157(1983).
3. J.S. Winfield et al., Phys. Rev. C 33, 1333(1986).
4. B. Berthier et al., Phys. Lett. 182B,15 (1986).
5. T. Tamura and K.S. Low, Comp. Phys. Commun. 8,349(1974).
6. H.G. Bohlen et al., Z. Phys. A322, (1985) 241.
7. N. Anyas-Weiss et al., Phys. Rep. 12C, (1974) 203.

G.M. Crawley, C. Djalali, A. Galonsky, A. Brown, N. Marty^a, M. Morlet^a, A. Willis^a

The study of spin excitations is important because it gives us information about the basic spin dependence of the nuclear force. Near a bombarding energy of 200 MeV, inelastic proton scattering at forward angles has been shown^{1,2} to be very selective of $l=0$ spin-flip excitations. There remain at least two interesting questions arising from these measurements: (1.) what can be learned from a comparison between the proton data and data obtained with different probes? and (2.) What is the source of the "quenching" of these transitions?

This report will discuss these questions, show some examples and present the current status of the inquiry into these issues.

Comparisons Between (p,p') and (e,e')

One of the initial problems in making comparisons between 1^+ states excited by inelastic proton scattering and inelastic electron scattering was the fact that the inelastic proton scattering appeared to see much more strength than inelastic electron scattering, particularly for broad states. Of course this problem could be the result of orbital and spin components interfering destructively in the electron scattering case. Since the problem appears to arise mainly for broad states, it seems more likely that the source of the difficulty is the different sensitivity of (p,p') and (e,e') reactions in selecting 1^+ states.

For the case of narrow states, there is rather detailed agreement between (p,p') and (e,e') in many cases although not in every case.

We have recently studied the isotopes ^{16}O and ^{18}O and a paper on these results will be published shortly³. Because they involve the

use of a gas cell, the oxygen isotopes present a technically challenging problem especially when one has to measure very forward angles. Our solution was to use a reasonably high pressure gas cell running at about 4 atmospheres with kapton windows. We measured and subtracted the contribution from the windows to obtain the oxygen spectrum. The best energy resolution obtained was 75 keV (full width half maximum). In particular the three previously known 1^+ states^{4,5} at 16.2, 17.1, and 18.8 MeV excitation energy are seen clearly in the spectrum.

The angular distributions for a number of states are shown in Figure 1, including the angular distributions for the three 1^+ states.

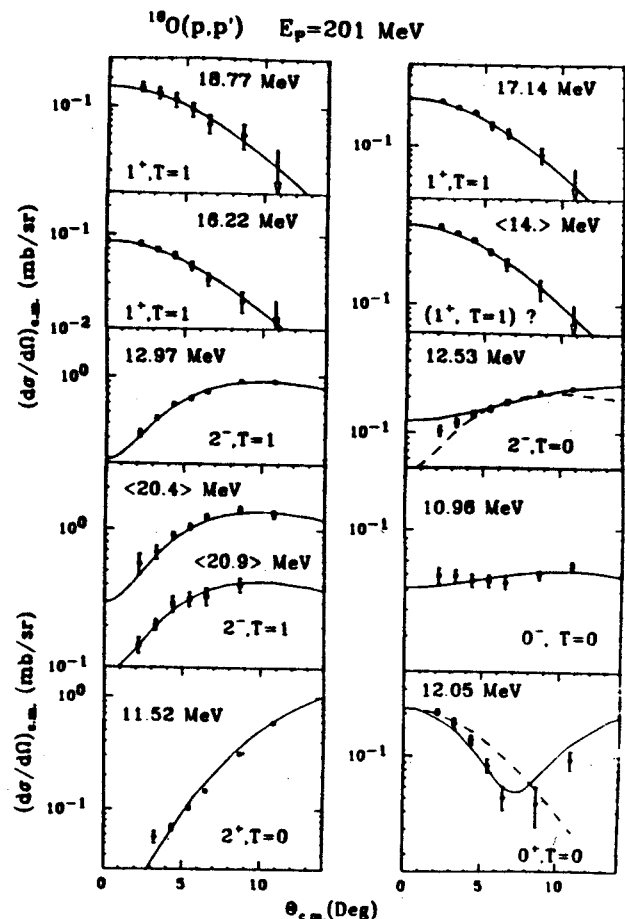


Fig. 1. Measured (p,p') angular distributions for some states in ^{16}O compared with microscopic DWBA calculations.

Obviously the angular distributions are quite characteristic of the ℓ transfer in this reaction. Even 1^+ and 0^+ states appear to be distinguishable since 0^+ states are characterized by a minimum in the angular distribution at around 7° with the cross section rising as one goes to larger angles while the cross section for 1^+ states continues to decrease with angle.

For the low-lying positive parity excitations in ^{16}O two-particle two-hole and four-particle four-hole excitations are most important. The only model space for which it is presently feasible to calculate these excitations allows for all configurations within the three orbits $1p_{1/2}$, $1d_{5/2}$ and $2s_{1/2}$ with a closed $(1s_{1/2})^4 (1p_{3/2})^8$ configuration for ^{12}C . The wave functions were obtained from a residual interaction⁶ determined by least squares fits to energy levels in the A=13-18 mass region.

The experimental results on M1 strength from (p,p') and (e,e') resemble one another more closely than the theoretical predictions resemble either of them. The only disagreements again occur for broad states. In the (e,e') measurements,⁴ there was some strength seen between 17 and 18 MeV which is not observed in the (p,p') measurements. On the other hand there is a state observed in (p,p') around 14.0 MeV which appears to be a 1^+ state although the analogue of such a state was not observed in the (p,n) reaction,⁷ and there are no known 1^+ states at this excitation energy. This region has not been studied by (e,e'). The $B(\sigma)$ values extracted from the (p,p') measurements are generally similar to the $B(M1)$ values except for the 16.2 MeV case where $B(\sigma)$ is much weaker.

The general conclusion from a number of detailed comparisons is that in many cases, particularly for narrow states, it is possible to extract separately the orbital and spin

pieces and to learn more about the detailed nature of the transitions. However there is still the second question raised earlier viz. the quenching of these M1 transitions observed in both (p,p') and (e,e').

Quenching

A number of possible explanations have been suggested to explain the quenching of spin-flip transitions. One possible explanation is that there may be experimental problems in obtaining the total strength of the 1^+ transitions. For example, the background may not be subtracted correctly or the states may be so small that it may be difficult if not impossible to observe them above the background. Certainly in the case of broad structures, background can be a significant problem.

In addition, there have been a number of theoretical mechanisms proposed to explain the quenching, viz core-polarization,⁸ configuration mixing, and mesonic effects,⁹ including the delta-hole interaction. This last effect acts mainly on the spin-isospin part of the interaction where $\Delta S=1$ and $\Delta T=1$. Normally one cannot readily separate $\Delta T=0$ and $\Delta T=1$ transitions. Only in a nucleus with a $T=0$ ground state and in which one can separate $T=0$ and $T=1$ excited states can one unambiguously separate $\Delta T=0$ and $\Delta T=1$ transitions. Therefore we have made a study of a number of sd shell nuclei ranging from ^{20}Ne to ^{32}S . Not only are there a number of $T=0$ nuclei available in the sd shell, but in addition very good shell model wave functions exist¹⁰ which allow good calculations of the cross section for 1^+ states to be made.

There is also a very noticeable difference in the quenching as one goes from the 15.11 MeV 1^+ , $T=1$ state of ^{12}C , where the quenching factor N is essentially unity,¹¹ to ^{48}Ca where N is equal¹² to 0.3. Therefore studies of sd shell nuclei allow one to obtain the quenching as a

function of mass between ^{12}C and ^{48}Ca . It should be stressed that when one is making a comparison with shell model wave functions it is not possible to make a precise state by state comparison, but rather it is more meaningful to compare the total summed strength predicted by the shell model with the total strength observed experimentally. The final motivation for studying sd shell nuclei is that in a number of cases both (γ, γ') ¹³ and (e, e') ¹⁴ measurements have been made in these nuclei and so it is possible to make a rather good comparison between the hadronic reactions and the electromagnetic ones.

Isoscalar and Isovector Transitions in 2s1d Shell Nuclei

Before discussing the individual nuclei in detail, there are a couple of general points to be made. First, the (p, p') reaction is very selective of 1^+ states under the kinematic conditions used. The second point is that the angular distributions are quite selective of the spin-parity as is seen in Fig. 2 where the angular distributions of a number of states in Mg^{24} are shown. It also appears that the angular distributions for 1^+ , $T=0$ and 1^+ , $T=1$ states are different. The 1^+ , $T=0$ states have a flatter angular distribution reflecting the slow variation of the isoscalar piece of the effective interaction with momentum transfer. However because the number of calibration cases is small this is not a very definitive means of selecting isospin. In addition, the isospin of a particular state may not be completely pure and this can also lead to some ambiguities. We shall discuss a few of the individual nuclei in turn.

A) ^{20}Ne & ^{22}Ne : The results from these isotopes have recently been published¹⁵ and will not be discussed further here.

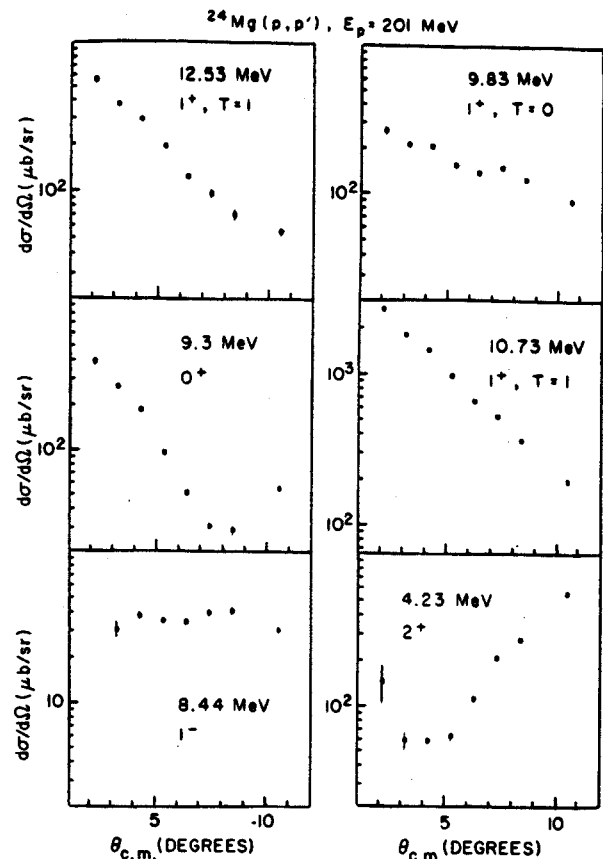


Fig. 2. Angular distributions for $^{24}\text{Mg}(p, p')$ for some representative states of different J^π , T .

B) ^{24}Mg : There are many 1^+ states seen in Mg^{24} . Using the angular distributions as a basis of making isospin assignments suggests that there are three $T=0$ states and seven $T=1$ states. If we compare the isoscalar and isovector strengths separately, we find that for isoscalar states $N=0.58$ and for isovector states $N=1.0$. However the isospin assignments are not unambiguous. In particular, the state at 9.83 MeV appears to be a 1^+ , $T=0$ state both from the (p, p') angular distribution and from the compilation of Endt and van der Leun¹⁶, but is seen in (e, e') . A state at 12.87 MeV has a slightly flatter angular distribution than a typical $T=1$ state but was nevertheless included¹⁶ in the $T=1$ states. If the total experimental strength is compared to the total predicted strength without regard to isospin, which is a much firmer number, the value of N obtained is $N=0.93$. (See Table I)

Table I: Values of $N = \frac{\sigma(\text{experimental})}{\sigma(\text{predicted})}$ for (p,p') reactions

Nucleus	N(T=1)	N(T=0)	N(Total)
²⁰ Ne	0.70-1.0	—	1.0
²⁴ Mg	1.0	0.58	0.93
²⁸ Si	0.70	0.50	0.68
³² S	0.83-1.02	0.52	0.96

C) ²⁸Si: The separation between T=0 and T=1 states is perhaps the cleanest in ²⁸Si. There is one known 1⁺ T=0 state, at 9.6 MeV, which is clearly seen in the present experiment¹⁷ although it is not resolved from a nearby 2⁺ state. The angular distribution is characteristic of a 1⁺ T=0 state except at backward angles where there is probably a contribution from the 2⁺ state. No other T=0 states are predicted above this energy. There are a large number of T=1 states observed and predicted. If one compares the predicted total strengths of T=0 and T=1 states, the value of N for isoscalar states is 0.50 and for the isovector states is 0.70, as given in Table I. Note that our previous publication¹⁷ had smaller values of N because of an error in the target thickness determination. If the total strengths are compared, an N of 0.68 is found.

D) ³²S: The nucleus ³²S has been well studied by electromagnetic probes^{13,18} and the analogue nucleus ³²P by the (p,n) reaction¹⁹. There are a number of interesting specific states which could be discussed including the known weak 1⁺, T=1 state at 7.00 MeV. Many candidates for 1⁺ states are seen in the (p,p') reaction in addition to four states identified as 1⁺ from the (γ,γ')¹³ and (e,e')¹⁸ reactions. A summary of the results for the 1⁺ states both for the (p,p') and the electromagnetic reactions is given in Table II. Particularly strong 1⁺ states seen in (e,e') at 11.12 and 11.63 MeV are also the strongest 1⁺ states observed in the (p,p') reaction at forward angles. The ratio of cross sections in (p,p') reactions is similar to

the ratio of B(M1) values extracted from the electromagnetic measurements. Overall we observed three states with ΔT=0 angular distributions and perhaps 12 states with ΔT=1 angular distributions. The state at 9.66 MeV seen in (e,e') and (γ,γ') appears to be a T=0 state on the basis of the (p,p') angular distribution.

Table II: Summary of Possible 1⁺ states in ³²S

E _x (p,p') (MeV)(a)	σ _{cm} (3°) (mb/sr)	E _x (γ,γ') (MeV)(b)	E _x (e,e') (MeV)(c)	Isospin (comments)
4.70	0.03			T=0
7.00	0.06			T=1
7.19	0.05			T=0
7.64	0.25			T=1
8.13	0.90	8.127	8.11	T=1
9.28	0.12	9.209	-	(T=0?)
9.66	0.15	9.661	9.68	T=1
9.94	0.29	-	(10.05)	(T=0?)
11.15	2.90	-	11.12	T=1
11.64	1.38	-	11.63	T=1
11.88	0.16			(1 ⁺ T=1,0 ⁺)
12.58	0.25			(1 ⁺ T=1,0 ⁺)
13.93	0.21			(1 ⁺ T=1,0 ⁺)
14.51	0.13			"
14.65	0.14			"
15.07	0.18			"
15.61	0.21			"

a) This work b) Ref 13 c) Ref 17

One puzzle is the fact that a reasonably strong 1⁺ state is seen at 7.64 MeV which is not observed in either of the electromagnetic measurements. Using the angular distributions as a guide to the isospin and including all possible 1⁺ states, the values of N obtained are N=0.52 for isoscalar states and N=0.83-1.02 for isovector states. The value of N without distinguishing T=0 and T=1 states and including all possible 1⁺ states is 0.96 (Table I).

Summary and Conclusions

The comparison of the results from (p,p') and electromagnetic measurements is very useful in providing further insights into the nature of particular transitions. It allows a stringent test of theoretical nuclear wave functions.

The quenching of 1^+ , T=1 states in the 2s1d shell nuclei is similar in both (p,p') and electromagnetic measurements. In most of the cases studied the value of N is close to unity with the exception of ^{28}Si .

While it is not possible to make a definitive statement about the T=0 strength, it appears that the quenching for these states is generally greater than for the T=1 states. This implies that Δ -nucleon hole mixing does not play a very strong role in the quenching of 1^+ states.

The quenching obtained without regard to isospin is also close to 1.0 for all the nuclei studied except ^{28}Si . From the systematics at the sd-shell Gamow-Teller beta decays, ^{20}Ne we would expect an overall quenching factor of about 0.6 for all of these sd-shell nuclei (^{20}He , ^{24}Mg , ^{28}Si and ^{32}S). Thus, the lack of quenching observed in these experiments is surprising, and may indicate some inaccuracy in the theoretical ground state wave function in these nuclei. It clearly is important to obtain accurate wave functions from more sophisticated calculations in heavier nuclei ($A > 40$) to make detailed comparisons with experimental results.

a. IPN, Orsay, France.

1. N. Anantaraman et al. Phys. Rev Letters 46, 1318(1981); G.M. Crawley et al Phys. Rev 26C,87(1982).
2. C. Djalali et al. Nuclear Physics A388, 1(1982).
3. C. Djalali et al. Submitted to Physical Rev. C (1986).
4. G. K uchler et al. Nucl. Phys. A406, 473(1983).
5. K.A. Snover et al. Phys. Rev C27,1837(1983).
6. B.S. Rehal and B.H. Wildenthal, Part. Nucl. 6, 137(1973); J.B. McGrory and B.H. Wildenthal, Phys. Rev. C7, 974(1973).
7. A. Fazely et al. Phys. Rev. C25, 1760(1982).
8. I.S. Towner and F.C. Khanna, Nucl. Phys. A399, 344(1983); G. F. Bertsch and I. Hamamoto, Phys. Rev. C26, 1323(1982); G.E. Brown et al. Nucl. Phys. A330, 290(1979); S. Krewald et al Phys. Rev Letters 46, 103(1981).
9. A. Bohr and B. Mottelson, Phys. Lett 100B, 10(1981); A. H arting et al. Phys Lett 104B, 261(1981); H. Sagawa and N. Van Giai Phys. Lett 113B, 119(1982).
10. B.A. Brown and B.H. Wildenthal Phys. Rev C28, 2397(1983).
11. J.R. Comfort et al, Phys Rev. C26, 1800(1982); J.R. Comfort et al. Phys Rev. C21, 2147(1980).
12. G.M. Crawley et al. Physics Letters 127B, 322(1983).
13. U.E.P. Berg et al. Phys Lett 140B,191(1984).
14. L.W. Fagg, Rev Mod Phys. 47, 683(1975).
15. A. Willis et al. submitted to Nuclear Physics (1986).
16. P.M. Endt and C. van der Leun, Nuclear Physics A310, 1 (1978).
17. N. Anantaraman et al. Phys. Rev. Letters 52, 1409(1984).
18. P.E. Burt et al. Phys. Rev C29, 713(1984).
19. B. Anderson et al. private communication.
20. B.A. Brown and B.H. Wildenthal, Atomic Data and Nuclear Data Tables, 33, 347(1985).

F.D. Becchetti,^a J. Jänecke,^a P. Lister,^a M. Dowell,^a A. Nadasen^b and J.S. Winfield

Data for $^{12}\text{C}(^7\text{Li},t)^{16}\text{O}$ at $E = 70$ MeV has been obtained at MSU-NSCL using the $K = 320$ spectrometer which permitted resolution (Fig. 1) of the low-lying levels of ^{16}O , in particular the $J^\pi = 1^-$ levels which are of great astrophysical interest (in the context of helium burning).¹ This permits extraction of the relative α -widths for these states. An initial analysis yields α -widths which appear to be consistent with values found³ using $^{12}\text{C}(^7\text{Li},t)$ at $E(^7\text{Li})=34$ MeV viz. $\gamma_\alpha^2(7.1)/\gamma_\alpha^2(6.9)\approx 0.2$ and $\gamma_\alpha^2(7.1)/\gamma_\alpha^2(9.6)\approx 0.4$. (The value of $\gamma_\alpha^2(7.1)$ determines the $^{12}\text{C}\rightarrow^{16}\text{O}$ rate in stars). The angular range covered was from 3° to 40° (lab). In addition, data obtained² earlier at IUCF ($E = 101$ MeV) has been analyzed, including identification of α -decay from levels at $E_x > 20$ MeV. Finite range DWBA analysis is in progress and some preliminary calculations for the 101 MeV data are shown in Fig. 2.

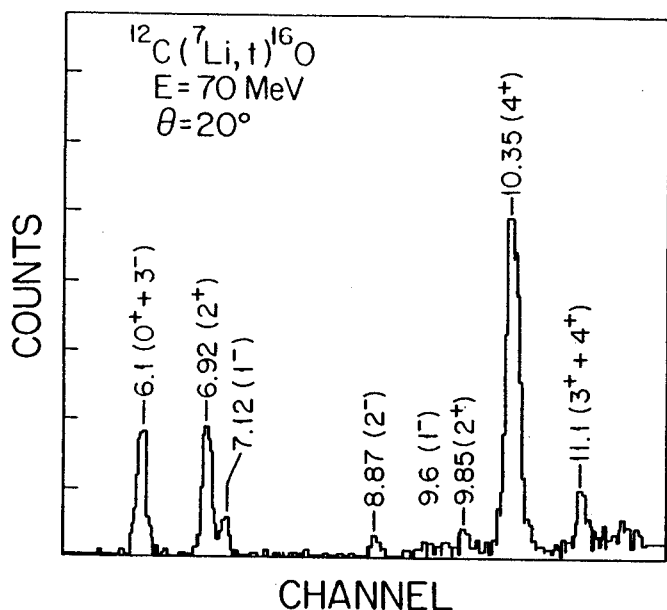


Fig. 1. A $^{12}\text{C}(^7\text{Li},t)^{16}\text{O}$ spectrum taken with the $K = 320$ spectrometer. Levels in ^{16}O are indicated by E_x (MeV) and J^π values.

- a. University of Michigan, Ann Arbor, MI
b. University of Michigan-Dearborn, Dearborn, MI

References

1. F.D. Becchetti, et al., Nucl Phys. A344, 336 (1980) and references cited therein.
2. F.D. Becchetti, et al., BAPS 31, 784 (1986).
3. F.D. Becchetti, E.R. Flynn, D.L. Hanson and J.W. Sunier, Nucl. Phys. A305, 293(1978).

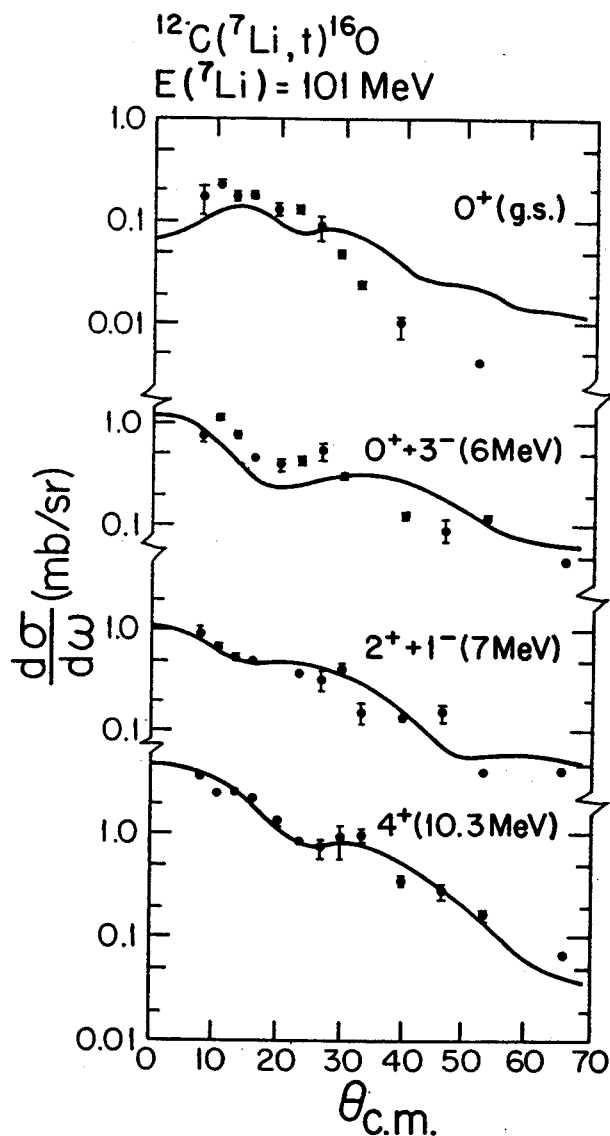


Fig. 2. Angular distributions for the $^{12}\text{C}(^7\text{Li},t)^{16}\text{O}$ reaction at 101 MeV. The curves are finite range DWBA predictions, normalized to the data.

S.M. Austin and E. Adamides

MSU-87-044

The spectrum observed at low momentum transfer in a typical (p,n) reaction is dominated by three excitations; the isobaric analog state (IAS), the giant Gamow Teller resonance, and the giant dipole (L=1) resonance. It is well known that the IAS contains almost all the Fermi strength and that the low lying Gamow Teller strength is about 60% of the sum rule limit. Much less is known about the dipole resonance and it exhibits what at first seems a rather puzzling property; it moves to lower excitation energy as the bombarding energy is increased. This behavior has been observed experimentally for all heavier systems investigated. The Zr isotopes have been studied in particular detail with the results shown in Fig. 1.

This behavior can be understood qualitatively as follows (See Fig. 2). Dipole (L=1) excitations in a charge exchange reaction are isovector in nature and can be accompanied by a spin transfer of S=0 or S=1. The S=0 strength is concentrated in a $J^\pi = 1^-$ state located at E_0 , the well known giant dipole resonance or GDR, while the S=1 strength leads

MSU-87-049

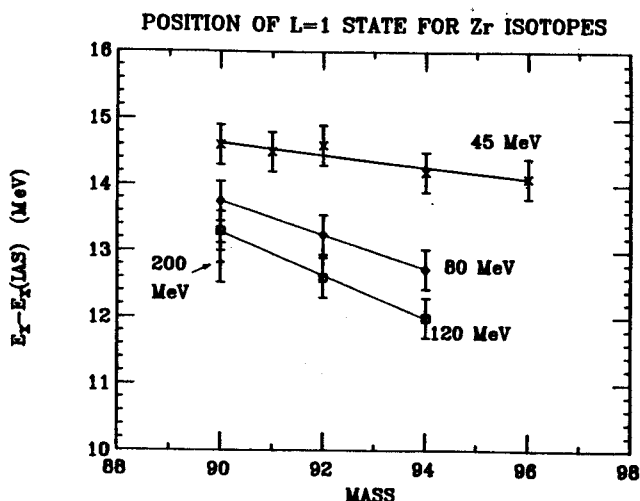


Fig. 1. Energies of the L=1 resonance for the Zn isotopes value are from Ref. 1.

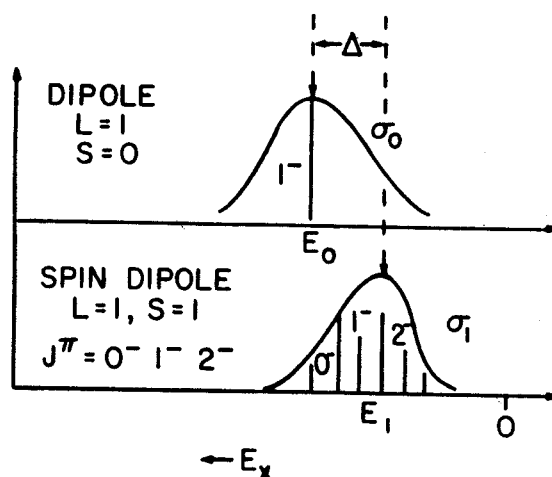


Fig. 2. Diagram showing assumed model and definition of terms.

to 0^- , 1^- , and 2^- states with centroid at E_1 . We call this excitation the giant spin-dipole resonance or GSDR. Because of the nature of the two body interaction mediating the transition, the S=0 excitation is dominant at energies near 45 MeV, but S=1 becomes much more probable, relative to S=0, as the proton bombarding energy increases toward 200 MeV. One then expects the centroid of the L=1 strength to move from E_0 toward E_1 with increasing energy. Rather general arguments² indicate that the S=0 GDR lies at higher excitation energy than the S=1 GSDR so this motion corresponds to a decreasing excitation energy. Detailed theoretical calculations³ qualitatively confirm this expectation.

We outline here a simple phenomenological description of this behavior, parametrized in terms of the positions E_0 and E_1 of the two resonances. This parametrization permits us to extract the splitting of the dipole and spin-dipole resonances and to locate the position of the GDR resonance from the (p,n) reaction studies, permitting a comparison with other techniques for exciting the dipole.

The position of the centroid of the L=1 excitations at a bombarding energy E_p is given by

$$C = \frac{\sigma_0 E_0 + \sigma_1 E_1}{\sigma_1 + \sigma_2} = E_0 - \frac{\sigma_1/\sigma_0}{1 + \sigma_1/\sigma_0} \Delta \quad (1)$$

where $\Delta = E_0 - E_1$ and $\sigma_0(\sigma_1)$ is the cross section for $S=0(S=1)$ transfer. It is possible to simplify this expression greatly if one knows the ratio σ_1/σ_0 . We assume here that this ratio is directly proportional to the ratio of the forbidden beta decay strengths, as is observed for the IAS and the Gamow Teller resonance in the L=0 case, namely

$$\sigma_1/\sigma_0 \approx N_D \left| \frac{V_{\sigma\tau}}{V_\tau} \right|^2 \frac{B(\text{GSDR})}{B(\text{GDR})} \quad (2)$$

Taddeucci, et al.⁴ have shown that $N_D |V_{\sigma\tau}/V_\tau|^2 = a^2 E_p^2$ where $a = 1/(55 \pm 1)/\text{MeV}$ and E_p is the bombarding energy. This relationship is accurate over the energy range of 45 to 200 MeV needed here. Assuming that the same relationship holds for L=1, one obtains

$$C = E_0 - \frac{\alpha a^2 E_p^2}{1 + \alpha a^2 E_p^2} \Delta \quad (3)$$

Here α is the ratio of the strengths $B(\text{GSDR})/B(\text{GDR})$. This ratio depends on the sum rule strengths for the transitions and the fraction of that strength found at low excitation. Further investigation will be required to obtain an accurate value of α ; for this initial work we assume that α is comparable to the analogous ratio for the L=0 transitions, $B(S=1, l=0)/B(S=0, l=0) \approx 1.5$, and take as an uncertainty ± 0.5 .

We then fit equation 3, with $\alpha = 1.0, 1.5,$ and 2.0 , to the data for the Zr isotopes in Fig. 1 with the results shown in Fig. 3 and Table 1. The data are well fitted by the equation for

these values of α . We note that in principle the results can be used to fix α . If one fits the Zr data with three parameters: α, E_0 and Δ , one obtains values of α near 1. Unfortunately the data are not sufficiently accurate to yield a precise value of α , but do appear to make values of $\alpha > 2$ unlikely.

Krmpotic, Nakayama and Pio Galeão² have discussed the nature of the giant first forbidden resonances and have given simple expressions for the excitation of the GDR and GSDR: the results for the GDR-GSDR splitting are given in Table 1.

E. Adamides greatly acknowledges the financial support given by the Academy of Athens-Greece from the V. Notara Bequest.

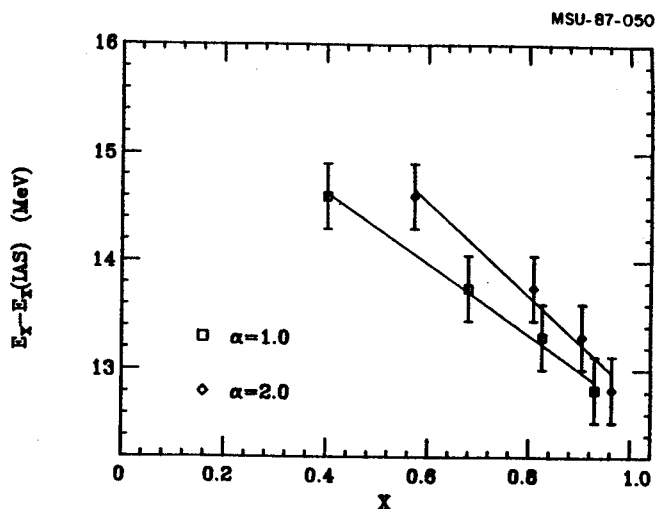


Fig. 3. Comparison of the resonance positions and Eq. 3. written as $C = E_0 - X\Delta$, where $X = \alpha a^2 E_p^2 / (1 + \alpha a^2 E_p^2)$. The straight lines are least square fits to the data.

Table 1.

References

Energy of the Dipole and the Dipole, Spin-Dipole Splitting

Nucleus	$E_o^{a)}$	$\Delta^{a)}$	$\Delta^{b)}$ theory
^{90}Zr	16.6 ± 0.9	3.9 ± 1.1	2.92
^{92}Zr	17.3 ± 1.3	5.3 ± 1.7	3.22
^{94}Zr	17.2 ± 1.4	5.9 ± 1.8	3.86

a) Calculated for $a = 1.5 \pm 0.5$

b) From Ref. 2.

1. W.A. Sterenburg, S.M. Austin, R.P. DeVito and A. Galonsky, Phys. Rev. Lett. 45, 1839(1980), and MSU Annual Report (1980) D.J. Horen et al, Phys. Lett 99B, 383(1981).
2. F. Krmpotic, N. Nakayama and A. Pio Galeao, Nucl. Phys. A399, 478(1983).
3. F. Osterfeld, S. Kruvald, H. Dermawan and J. Speth, Phys Lett 105B, 257(1981).
4. T.N. Taddeucci, et al., Phys. Rev. C25, 1094(1981).

MEASUREMENT OF THE RECOIL POLARIZATION OF ${}^6\text{Li}^*$ (2.186 MeV, 3+)
USING A MULTI-PSD ARRAY

R. Aryaeinejad, W.R. Falk^a, D. Steski^a, O. Abou-Zeid^a,
A. Mirzai^a, and J.R. Campbell^b

The measurement of particle-particle angular correlations in a nuclear reaction can give us useful information regarding the reaction mechanism, as well as information on the spin, parity, and polarization of the recoil nucleus. The spin and parity of the intermediate state determine the maximum rank of the tensor moments involved¹. In general, the recoil breakup distributions have to be measured in several planes in order to extract the complete set of even-rank (if polarization axis is chosen perpendicular to the reaction plane) tensor moments describing the polarization.²

The recoil polarization of ${}^6\text{Li}$ (2.186 MeV, 3+) has been investigated by measurements of the angular correlations between particles α_1 and α_2 produced in the sequential reaction ${}^9\text{Be}(p, \alpha_1){}^6\text{Li}(3+) \rightarrow \alpha_2 + d$ at α_1 scattering angles of 20, 30, 45, and 60 degrees (lab.), and a proton bombarding energy of 40 MeV from University of Manitoba sector-focused cyclotron. The measurements were made using a two-armed detection system. The α_1 -particles were detected using a three element ΔE (100 μm), PSD (1000 μm), and V (200 μm , to veto energetic protons) particle telescope. The second arm consisted of four 8x47 mm position sensitive detectors (PSD's) in a cross configuration, two (right and left) mounted with their long axis parallel to the reaction plane and the other two (top and bottom) mounted perpendicular to the reaction plane, and a central ΔE -E-V telescope ($\Delta E=200$ μm , $E=1000$ μm , and $V=1000$ μm) covering the gap between the four PSD's. All PSD's had a thickness of 100 μm except for the bottom PSD which had a thickness of 500 μm . With this arrangement we were able to record the recoil distributions in both horizontal and vertical

planes simultaneously. A collimator with four 1 mm bars in front of each PSD was used for position calibrations. A Be foil of thickness 85 $\mu\text{g}/\text{cm}^2$, was used as a target. Figure 1 shows a two-dimensional position versus energy spectrum for the right PSD at $\theta(\alpha_1) = 60$ degrees (lab.). Both alpha locus (right parabola) and deuteron locus (left parabola) from $\text{Li}(3+)$ breakup can be seen in this figure. The analysis of the event-recorded data reconstructs the center of mass breakup angles for the ${}^6\text{Li}^* \rightarrow \alpha + d$ decay for each detected coincidence event. An appropriate frame of reference is defined by selecting the x-axis along the direction of the recoiling ${}^6\text{Li}^*$ nucleus and the z-axis perpendicular to the reaction plane. In

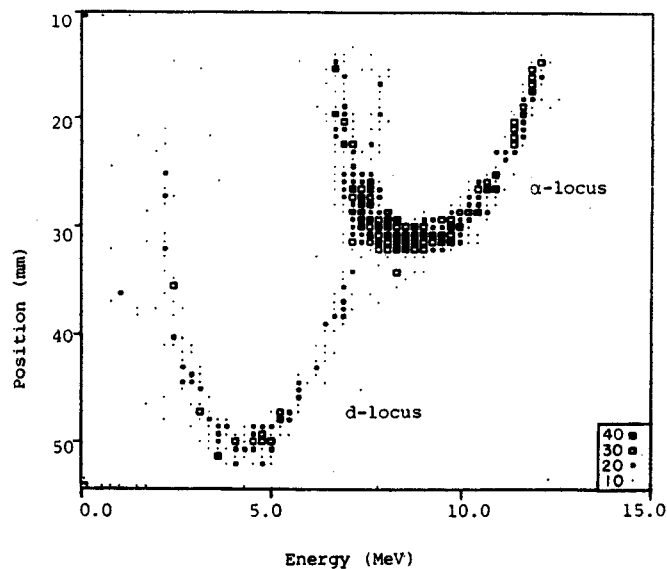


Fig. 1. Position-energy recoil locus for the right PSD, extracted at $\theta_\alpha = 60$ degrees.

this frame (with θ and ϕ the cm angles) the 'top' PSD detector measures events in the neighborhood of $\phi=0$ or π and $0 < \theta < \pi/2$. The 'right' PSD detector measures events in the neighborhood of $\theta=\pi/2$ and $\pi < \phi < 2\pi$. Figure 2-a is a θ - ϕ plot of the experimental results where the

angle of the α -particle was 30° .

Monte Carlo simulations were performed by calculating events subject to all the geometrical constraints of the experiment. These events were then analyzed in a manner identical to the experimental data itself. The results corresponding to the data of Fig. 2-a are shown in Fig. 2-b. This calculation assumed, for simplicity, the isotropic breakup of ${}^6\text{Li}^*$, and hence would not be expected to represent the data in detail. What Fig. 2-b

does show, however, is that the geometric bounds of the angles are very well reproduced in the simulation.

Further Monte Carlo calculations are now being made describing each of the different possible terms in the breakup of ${}^6\text{Li}^*$. A linear combination of these terms will then be fitted to the data in order to extract the statistical tensor t_{kq} .

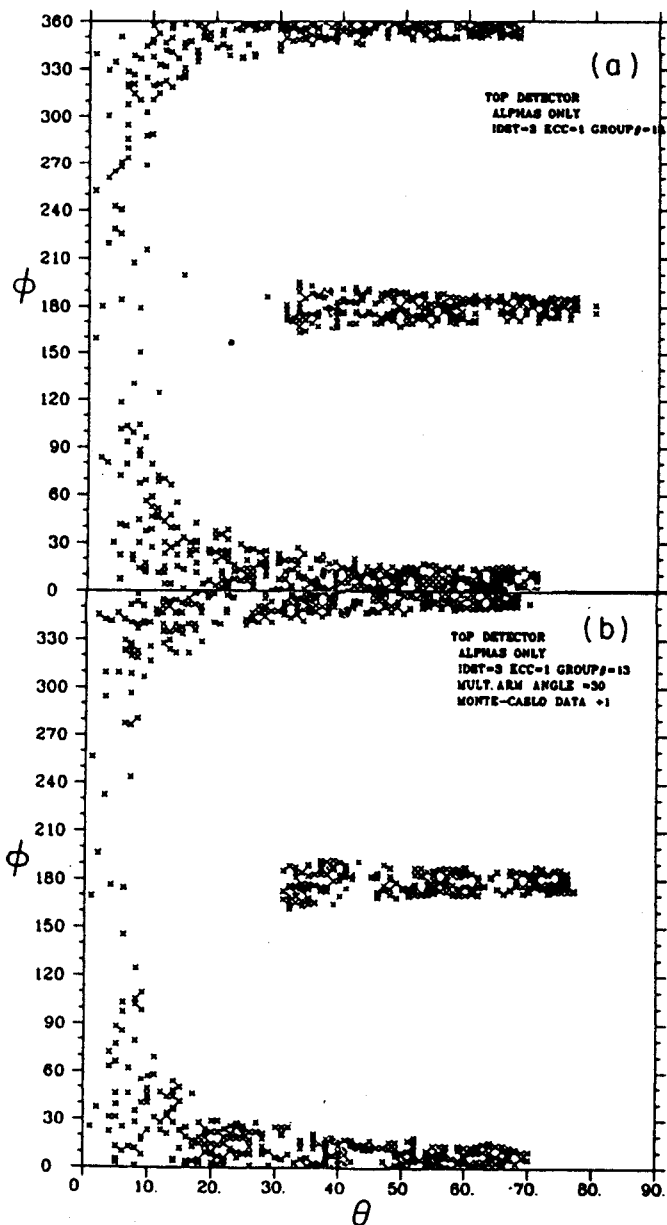


Fig. 2. (a) θ - ϕ plot of experimental data recorded at $\theta_\alpha = 30^\circ$ in the top PSD, (b) Monte Carlo simulated events for the same conditions as above.

- a. Department of Physics, University of Manitoba, Winnipeg, Canada.
- b. Institut für Physik der Universität Basel, Basel, Switzerland

References

1. M. Simonius, Lecture Notes in Physics, Vol. 30, Springer, Berlin, p. 38(1974).
2. N.S. Zelenskaya and I.B. Teplov, Nucl. Phys. A406, 306(1983).

R. Madey^a, B.S. Flanders^a, B.D. Anderson^a, A.R. Baldwin^a, C. Lebo^a, J.W. Watson^a,
S.M. Austin, A. Galonsky, B.H. Wildenthal^b and C.C. Foster^c

Studies of the (p,n) reaction at energies above 100 MeV yield unique information about spin strength in nuclei: the selectivity of the reaction for spin transfer and the existence of a strong sum rule allow a rigorous confrontation of experiment and theoretical expectations. Typically 60% of the sum rule strength is found in the low excitation energy region with the remainder presumably shifted to higher excitation energies.

The sd shell nuclei form an ideal site for more detailed (p,n) studies. Full sd shell wavefunctions have been obtained¹ and provide an accurate description of the level energies and other observables. In particular, predictions of the Gamow Teller (GT) strength are available and can be compared with the (p,n) measurements. At low excitation, the level spacing often allows a level by level comparison; at higher excitation energies, comparisons can be made in an average sense. In the particular case of $^{26}\text{Mg}(p,n)^{26}\text{Al}$, one can make a reasonably clean classification of the transitions by their isospin. One finds that the strength to T=0 states is relatively insensitive to details of the model (e.g. the amount of configuration mixing) and hence provides a sharp test of quenching of the spin transitions. On the other hand, the T=2 transitions, while making up a minor part of the overall transition strength are particularly sensitive to configuration mixing and provide a good test of the shell model calculation itself. Earlier work on this reaction at lower energy or with lower resolution is described in references 2-4.

The experiment was performed at 134.4 MeV using the beam swinger facility of the Indiana University Cyclotron Facility. Neutrons were detected in three large (1.02 m long by 0.508 m

high by 10.2 cm thick) mean-timed neutron detectors placed 85.8 ± 0.2 m from the target. The overall time resolution was 730 psec, corresponding to an energy resolution of 370 keV for E_n near 130 MeV. Absolute cross sections were extracted with efficiencies calculated with the Monte Carlo code of Cecil, et al⁵; the overall normalization uncertainty is $\pm 13\%$. A spectrum is shown in Fig. 1.

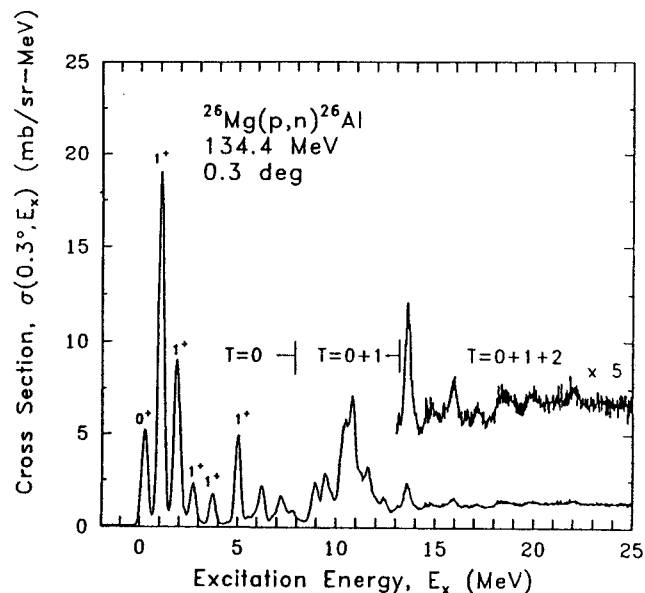


Fig. 1. Excitation-energy spectrum of the $^{26}\text{Mg}(p,n)^{26}\text{Al}$ reaction. Regions where states of different isospins occur are noted. The insert is scaled up by a factor of five.

Figure 1 also shows the allowed isospins. Thus states observed up to $E_x = 8$ MeV are pure T=0. At higher excitation the situation is more complex, but one can get an idea of the isospin concentration by examining the shell model calculations. They indicate that in the region of excitation from 8 to 13.3 MeV 78% of the strength is T=1 and 22% T=1. They also indicate that there is a strong T=2 excitation near 13.3 MeV. Energy systematics, based on the mass of

²⁶Na and the Coulomb energy systematics indicate that the lowest T=2 state in ²⁶Al lies at 13.55 ± 0.06 MeV. We observe a strong peak at 13.6 MeV and based on the above evidence assign this transition as T=2.

The GT transition strengths were obtained by normalization to the strengths known from β decay of the lowest four 1⁺ states in ²⁶Al. The resulting strengths in the regions of excitation energy 0 to 8 MeV, 8.0 to 13.3 MeV and 13.3 MeV to 15 MeV are B(GT)=2.54, 1.57 and 0.30, respectively, in units where the GT strength for the decay of the neutron is 3. The 13.6 MeV transition has B(GT)=0.12. In order to compare these strengths to the sum rule: $\sum B(GT, \beta^-) - \sum B(GT, \beta^+) = 3(N-Z) = 6$, one needs an estimate of the β⁺ strength. The shell model predicts $\sum B(GT, \beta^+) = 1.78$. The observed overall strength compared to the sum rule is then $(2.54+1.57+0.30)/(6+1.78)=0.57$. I.e. 57% of the sum rule strength is observed, comparable to that found in other nuclei.

A comparison for the T=0 transitions in the region of excitation below 8 MeV to the shell model predictions yields $B(GT, \text{expt}, <8 \text{ MeV}) / B(GT, \text{th'y}) = 0.63$. Finally the predicted strength of the 13.6 MeV transition is 0.08, somewhat weaker than observed.

The results are summarized in Table 1. The second column contains the predictions for the pure jj coupling limit and the third column the full sd shell prediction. A comparison of these

columns shows the relative sensitivity to configuration mixing. As noted above transitions to the T=2 states are particularly sensitive differing by a factor of 3.6. Column 4 of the table also makes clear the concentration of the GT strength below $E_x = 15$ MeV. Finally, the last two columns compare the theoretical prediction, quenched by a factor of 0.57, with the experimental results. The last column has been obtained by weighting the experimental results in the isospin mixed regions by the predicted ratios of strength. Finally Fig. 2 shows the GT strength lying below a given E_x . It is clear that the shell model provides a good overall description of the experimentally observed strengths.

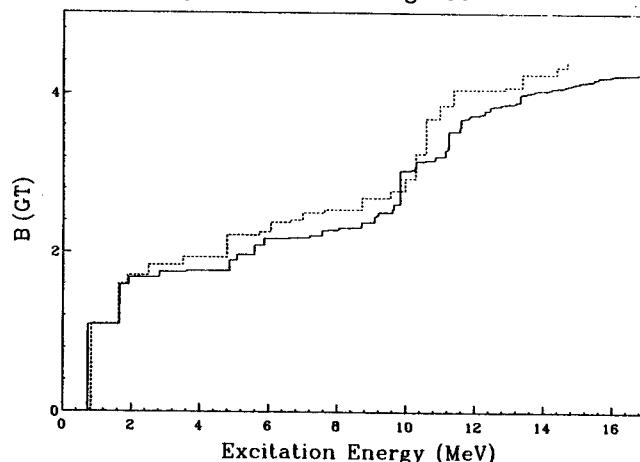


Fig. 2. The accumulating sum of the GT strength below a given excitation energy in ²⁶Al. The dashed line gives the experimental results and the solid line the theoretical predictions scaled by a factor of 0.57. Energies are plotted relative to the isobaric analog state.

Table 1. Gamow Teller Strength for ²⁶Mg → ²⁶Al

T	B _{jj,fn} (GT) (total)	B _{th,fn} (GT) (total)	B _{th,fn} (GT) (E _x < 15 MeV)	B _{th,0.57} (GT) (E _x < 15 MeV)	B _{pn} (GT)
0	6.533	4.887	4.765	2.70	2.95
1	4.800	2.598	2.331	1.32	1.33
2	1.067	0.297	0.165	0.09	(>0.12) (<0.30)
Sum	12.400	7.782	7.261	4.12	

- a. Kent State University, Kent, Ohio
- b. Drexel University, Philadelphia, PA
- c. Indiana University Cyclotron Facility,
Bloomington, IN

References

1. B.H. Wildenthal, Bull. Am. Phys. Soc. 27,
725(1982); Progress in Particle and Nuclear
Physics 11, 5(1984).
2. C.D. Goodman, et al, Nucl. Phys. A374,
241c(1982).
3. W.A. Sterrenburg, S.M. Austin, U.E.P. Berg
and R. DeVito, Phys. Lett. 91B, 337(1980).
4. U.E.P. Berg, S.M. Austin, R. DeVito, A.I.
Galonsky and W.A. Sterrenburg, Phys. Rev.
Lett. 45, 11(1980).
5. R.A. Cecil, B.D. Anderson and R. Madey,
Nucl. Instr. and Meth. 161, 439(1979).

J. Duffy^a, G.M. Crawley, J. van der Plicht^b, O. Scholten^c, J. Finck^d,
 R.S. Tickle^e, S. Gales^f and C.P. Massolo^g

A preliminary report of this work was given in last years Annual Report. The details of the experimental technique and the analysis were given in that report and will therefore not be repeated. Instead we will focus on the results, particularly for the high-lying regions of the Europium and Samarium isotopes and comparisons with theoretical predictions. This work is presently being prepared for publication.

Spectra from the (α, t) reaction on $^{144,148,152,154}\text{Sm}$ targets at 7° are displayed in Fig. 1(a). All four spectra show a broad structure (labelled A) which occurs at a slightly higher excitation energy than a pronounced minimum in each spectrum. The broad structure occurs at a Q-value of around -23 MeV in ^{145}Eu , corresponding to $E_x = 6.4$ MeV. As the deformation increases from ^{145}Eu to ^{155}Eu , the structure "A" moves closer to the corresponding ground state. There is also a second broad structure (labelled B) in all the spectra. The maximum of this structure occurs at a Q-value of about -32 MeV in ^{145}Eu ($E_x = 15$ MeV). This structure also moves closer to the corresponding ground state as the deformation increases but remains in the unbound region of the spectrum in all four Europium isotopes.

Cross section angular distributions were obtained by "slicing" the spectra from about 2 MeV to about 15 MeV excitation energy in 520 keV wide bins. These cross sections were then fitted by mixtures of l -transfers calculated in the DWBA and using the minimum χ^2 procedure described earlier. The l -values used in the fit were those suggested by the Nilsson model viz. $l = 3, 5, \text{ and } 6$ for $^{145, 149}\text{Eu}$ and $l = 2, 3, 5$ and 6 for $^{153, 155}\text{Sm}$. In fact no $l = 2$ strength was found probably because the cross sections for l

$= 2$ are much smaller than those for the other l -values. Some examples of the fits obtained using this procedure are shown in Fig. 2. The excitation energies shown in this Figure are those at the center of the slice. Generally the fits were quite good, the only exception being near the 9° region in ^{153}Eu where the measured cross section appears to be high. However the inclusion of this point had little effect on the conclusions and so it was included. In most cases, mixtures of different l -values gave the best fit but in some cases a single l -value gave the minimum χ^2 .

However if one examines the χ^2 values for other combinations of l -transfers, apart from the one which gives the minimum χ^2 one finds that the χ^2 minimum is generally not very sharp. For example, for a slice centered at 7.18 MeV in ^{153}Eu , the minimum χ^2 value is 3.6 for a combination of l -transfers of 6 and 3. But there are 8 other combinations of l -transfers which have χ^2 values less than twice the minimum value. This leads to some ambiguity in the l -values and the corresponding C^2S values extracted at each excitation energy. Such a situation is typical for much of the high excitation energy region and makes it difficult to draw definite conclusions about the strength for a particular l or j value.

However if one uses the minimum χ^2 procedure to extract the summed strengths up to about 15 MeV excitation energy, we find that in general a substantial fraction of the sum rule limit is obtained. In ^{145}Eu , the agreement with previous work is reasonably good. For ^{149}Eu and ^{155}Eu , the $l = 5$ and $l = 6$ strengths are close to unity given the fairly large uncertainties. The $l = 3$ strength is greater than the sum rule

limit, but presumably both $j = 5/2$ and $j = 7/2$ components are present so that the limit in this case should be 2. For ^{153}Eu , the amount of $l=6$ strength seen is rather small but the $l=5$ strength exceeds the sum rule limit by a factor of two. This leads one to suspect that some $l=6$ strength has been misidentified as $l=5$, perhaps because of the poor fits near 9° .

Spectra from the $(\alpha, ^3\text{He})$ reaction on $^{144,148,152,154}\text{Sm}$ targets at 7° are displayed in Fig. 1(b). All four spectra show a broad structure (labelled A) which occurs at a Q-value of about -25 MeV ($E_x = 11$ MeV) in ^{145}Sm and at about -20 MeV ($E_x = 5$ MeV) in ^{155}Sm . As was the case in the Europium nuclei, this broad structure moves closer to the ground state in the Samarium isotopes as the deformation increases. The structure therefore occurs in the unbound region in $^{145,148}\text{Sm}$ and in the bound region in $^{153,155}\text{Sm}$. The width of the structure also appears to decrease as the deformation of the nucleus decreases.

Cross section angular distributions were obtained as for the Europium isotopes by "slicing" the spectra in 520 MeV wide bins. A similar analysis to that described for the Europium isotopes was carried out using a χ^2 minimization procedure the only difference being the possible l -transfers allowed. In $^{145,149,153}\text{Sm}$, since the sum of the C^2S values for $l=5$ ($1h\ 9/2$) exceeds the sum rule limit for the low lying states, this l -value was excluded and only $l=1, 3, 4, 6$ and 7 were used in the fitting procedure. For ^{155}Sm $l=5$ was also included. Some examples of the fits obtained using the χ^2 minimization procedure are shown in Fig. 3. The excitation energies indicated are those at the center of the energy slices. In almost all cases, the fits are excellent. The corresponding χ^2 values are close to one except for the highest excitation energy region, above about 12 MeV, where the χ^2 values increase sharply at least for the three heavier isotopes. However in spite of the excellent quality of the

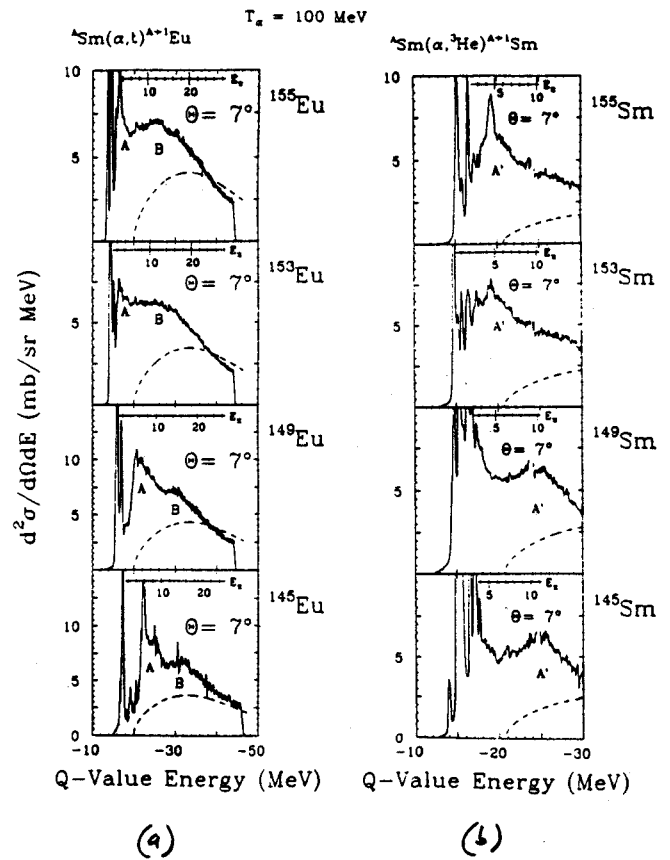


Fig. 1. a. Triton spectra at 7° for proton states excited in the $^{141,148,152,154}\text{Sm}(\alpha, t)^{145,149,153,155}\text{Eu}$ reactions.

b. ^3He spectra at 7° for neutron states excited in the $^{144,148,152,154}\text{Sm}(\alpha, ^3\text{He})^{145,149,153,155}\text{Sm}$ reactions.

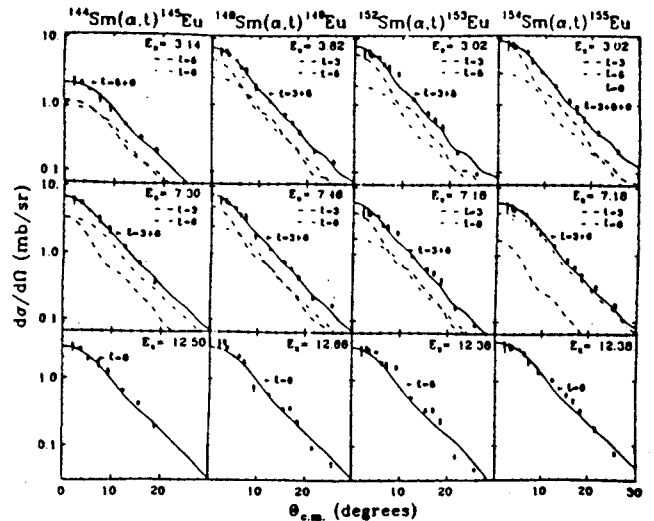


Fig. 2. Angular distributions of some high-lying regions in $^{145,149,153,155}\text{Eu}$ after background subtraction. Each region is 520-keV wide, centered at the excitation energy E_x (in MeV) indicated. The curves are the minimum- χ^2 fits using the DWBA.

fits, there is still some uncertainty in the precise l -assignments because of the similarity of the angular distributions.

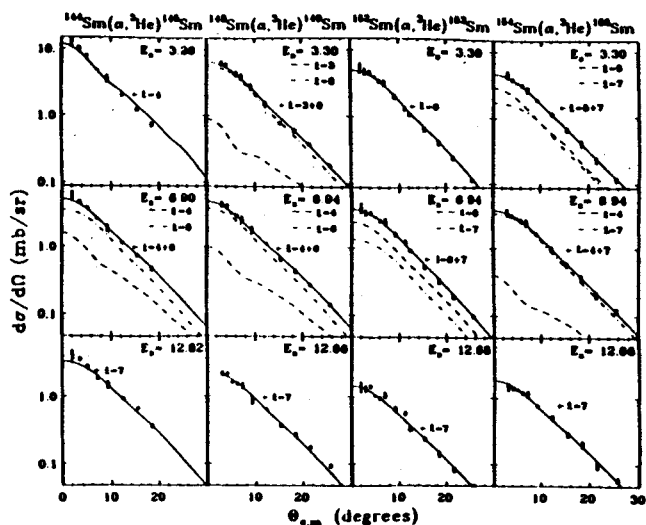


Fig. 3. Angular distributions of some high-lying regions in $^{145,149,153,155}\text{Sm}$ after background subtraction. The curves are the minimum χ^2 fits using the DWBA angular distributions. The l -values determined by this procedure are indicated.

Little $l=3$ strength is seen in any of the nuclei and little $l=4$ strength is seen in ^{153}Sm and ^{155}Sm . Some $l=4$ strength is extracted for the ^{149}Sm and ^{145}Sm at low excitation energy but these numbers are probably not very reliable. There is substantial (approximately equal to the sum rule) $l=6$ strength observed in ^{145}Sm , ^{149}Sm and ^{153}Sm and a small amount of $l=7$ strength mainly at high excitation. For ^{155}Sm , a small amount of $l=5$ strength is seen and rather less $l=6$ strength. However, the sum of the $l=6$ and $l=7$ strengths is similar to that seen in the other three nuclei and some $l=6$ strength may have been misidentified as $l=7$.

Theoretical spectra were obtained by starting with the predicted strength distributions from the quasi-particle phonon model (QPPM) ¹ for the particular j values included in the theory, and converting them, using the DWBA calculations, into a double differential cross-section (mb/sr MeV).

For ^{145}Eu , the j -values used were $2f_{7/2}$, $1h_{9/2}$ and $1i_{13/2}$. The comparison between the

background-subtracted experimental spectra and the theoretical spectra at 2° , 7° and 12° for ^{145}Eu are shown in the left panels of Fig. 4. (The excitation energy range from 0 to 1.5 MeV is not plotted, as it is dominated by orbitals not included in the theoretical spectrum.) There is good agreement at all three angles. This demonstrates the validity of the QPPM model and confirms the strong overlap between the $2f_{7/2}$, $1h_{9/2}$ and $1i_{13/2}$ proton strength functions in the energy range from 3 MeV to about 11 MeV. The width of the predicted strength distribution is similar to but slightly smaller than the experimental one. This may indicate that the damping of the high-lying orbitals considered is slightly smaller experimentally than is predicted theoretically. The excess experimental cross section seen at all three angles for $E_x > 10$ MeV may be due to some orbital(s) not included in the theoretical spectrum.

A comparison was also made (Fig. 4) between the experimental spectra (background-subtracted) taken at 2° , 7° and 12° for $^{153,155}\text{Eu}$ and the corresponding theoretical spectra were obtained by adding up the contributions of the predicted $3s_{1/2}$, $2d_{5/2}$, $2d_{3/2}$, $2f_{7/2}$, $1g_{7/2}$ and $1h_{11/2}$ strength distributions. The low l -transfers ($l=0$ and $l=2$) contributed only about 10% to the total predicted cross section. Unlike the ^{145}Eu case, the plots for $^{153,155}\text{Eu}$ in Fig. 4 extend down to $E_x = 0$ MeV. As in the ^{145}Eu case, the theoretical cross sections generally have the same magnitude as the experimental cross sections at all angles for low excitation energies, but there is a marked (and systematic) disagreement for excitation energies above 3 MeV. This is very likely due to the neglect of the $1h_{9/2}$ and $1i_{13/2}$ strength distributions in the theoretical spectra, both of which would have made substantial contributions to the spectra.

Similar comparisons were made for the predicted neutron strength distributions for the

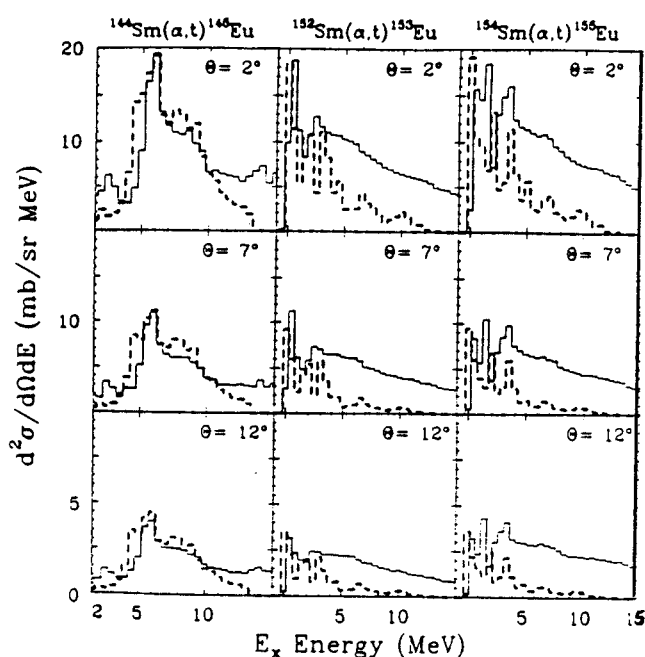


Fig. 4. Comparison between the background subtracted experimental spectrum (solid histogram) for proton states in $^{145}, ^{149}, ^{153}, ^{155}\text{Eu}$ and the predicted spectrum (dashed histogram) obtained by the conversion of theoretical strength functions at three angles.

nuclei ^{153}Sm and ^{155}Sm . (Predictions were not available for ^{145}Sm and ^{149}Sm). Theoretical spectra were obtained at angles of 3° , 7° and 12° by adding up the contributions of the $3p_{1/2}$, $3p_{3/2}$, $2f_{5/2}$, $2f_{7/2}$, $2g_{9/2}$, $1h_{9/2}$ and $1i_{13/2}$ strength distributions. The $\ell=1$ cross section from the $3p_{1/2}$ and $3p_{3/2}$ strengths is only about 2% of the total theoretical cross section. In Fig. 5, the theoretical spectra at the three angles are compared with the corresponding background-subtracted experimental spectra. The theoretical spectra have somewhat higher cross sections than the experimental spectra at very low excitation energies ($E_x < 1$ MeV), about the same cross sections for $E_x = 2-5$ MeV and considerably less cross sections for $E_x > 5$ MeV. The excess experimental cross section occurring for $E_x > 3$ MeV may represent the contribution of the $1j_{15/2}$ neutron excitation. Until a calculation is made, which includes the $1j_{15/2}$ strength it would be premature to draw conclusions about the spreading widths of individual single-particle excitations.

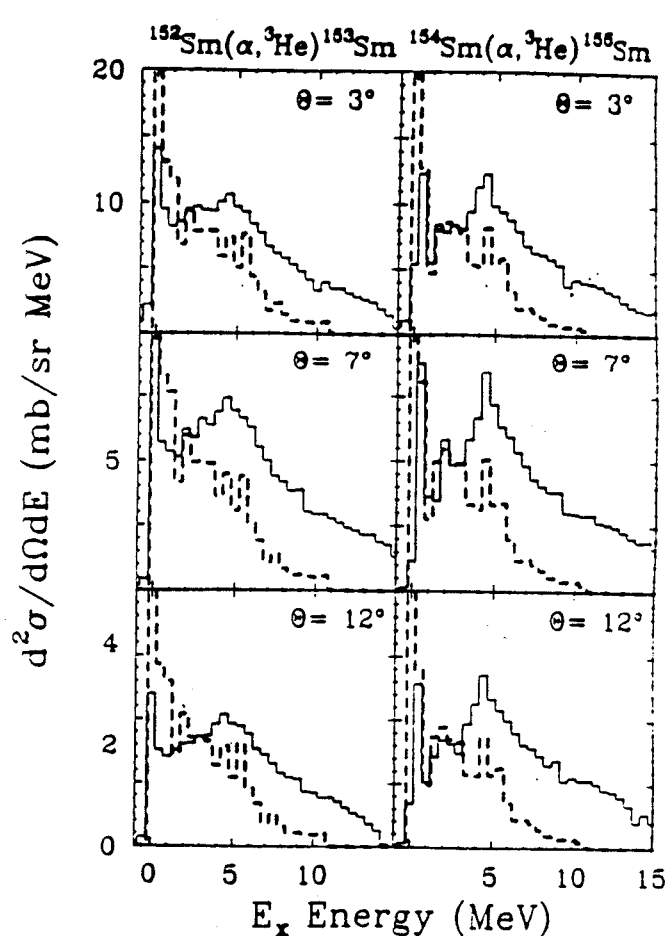


Fig. 5. Same as Figure 4 applied to the high-lying neutron states in $^{153}, ^{155}\text{Sm}$.

- a. Hughes Aircraft Company, Los Angeles, CA
- b. University of Groningen, The Netherlands
- c. K.V.I., Groningen, The Netherlands
- d. Central Michigan University, Mt. Pleasant, MI
- e. University of Michigan, Ann Arbor, MI
- f. IPN Orsay, France
- g. University of La Plata, Argentina

References

1. V.G. Soloviev, Ch. Stoyanov and A.I. Vdovin, Nucl. Phys. **A342**, 261(1980) Ch. Stoyanov and A.I. Vdovin, Phys. Lett. **130B**, 134(1983).

J. Batchelder and Wm.C. McHarris

We have reinvestigated the decay of ^{107}Cd (as an undergraduate research project) to obtain information on the weaker γ rays. ^{107}Ag lies three proton holes below the $Z = 50$ shell, and the recent availability of precise shell-model calculations¹ warrants a closer look at these states. In addition, many of the low-lying negative-parity states in nearby nuclei have been found to be collective, providing another reason for investigating them.

Samples of 6.5-hr ^{107}Cd were prepared by neutron bombardment of highly-enriched (>96%)

^{106}Cd in the MSU Triga reactor. Cumulative singles γ -ray spectra were taken as follows: Six spectra during the first half-life of a sample, then spectra at 6.5-hr intervals until essentially no ^{107}Cd peaks could be seen. Corresponding spectra from the different bombardments were summed and analyzed by the peak-analysis program Phaedrus. An example of a singles spectrum is shown in Fig. 1 -- it consists of the summed spectra for the first 26 hours from five bombardments, i.e., a total of 130 hours. It shows the positions of most of

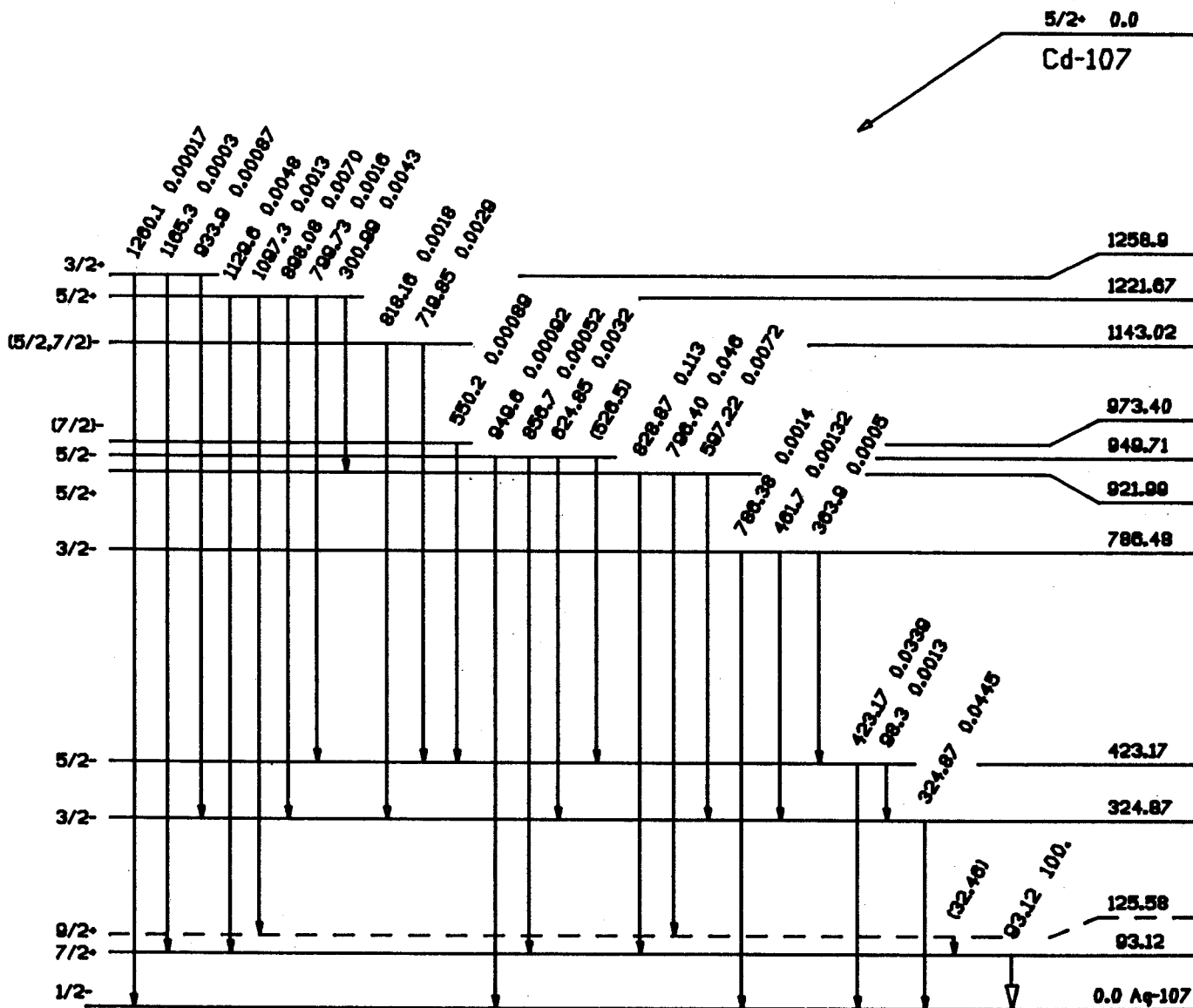


Fig. 1. Summed 130-hr γ -ray spectrum from the decay of ^{107}Cd .

the major ^{107}Cd peaks, plus the major contaminants.

The principal contaminants were found to be ^{115}Cd and ^{117}Cd . We compensated for these and for the background peaks by a careful cross-comparison with time. A list of the γ rays we attribute to ^{107}Cd decay is given in Table 1, together with their intensities and a comparison with previous results^{2,3}.

A preliminary level scheme is shown in Fig. 2. We confirmed most of the previously reported peaks, and have added a 364.0-keV peak. Previously reported states at 1326 and 1390 keV

were not confirmed. Nor was the $9/2^+$ state at 125.58 keV, for its 2.5-keV deexciting transition lies below our threshold. A careful analysis of the "unknown" peaks in the spectra is now underway, some of which may belong to ^{107}Cd decay. Our shell-model analysis is also in progress.

References

1. B. A. Brown, NSCL, private communication.
2. T. Paradellis and C. A. Kalfas, *Z. Phys.* **271**, 79 (1974).
3. M. Harmatz, *Nucl. Data Sheets* **38**, 656 (1981).

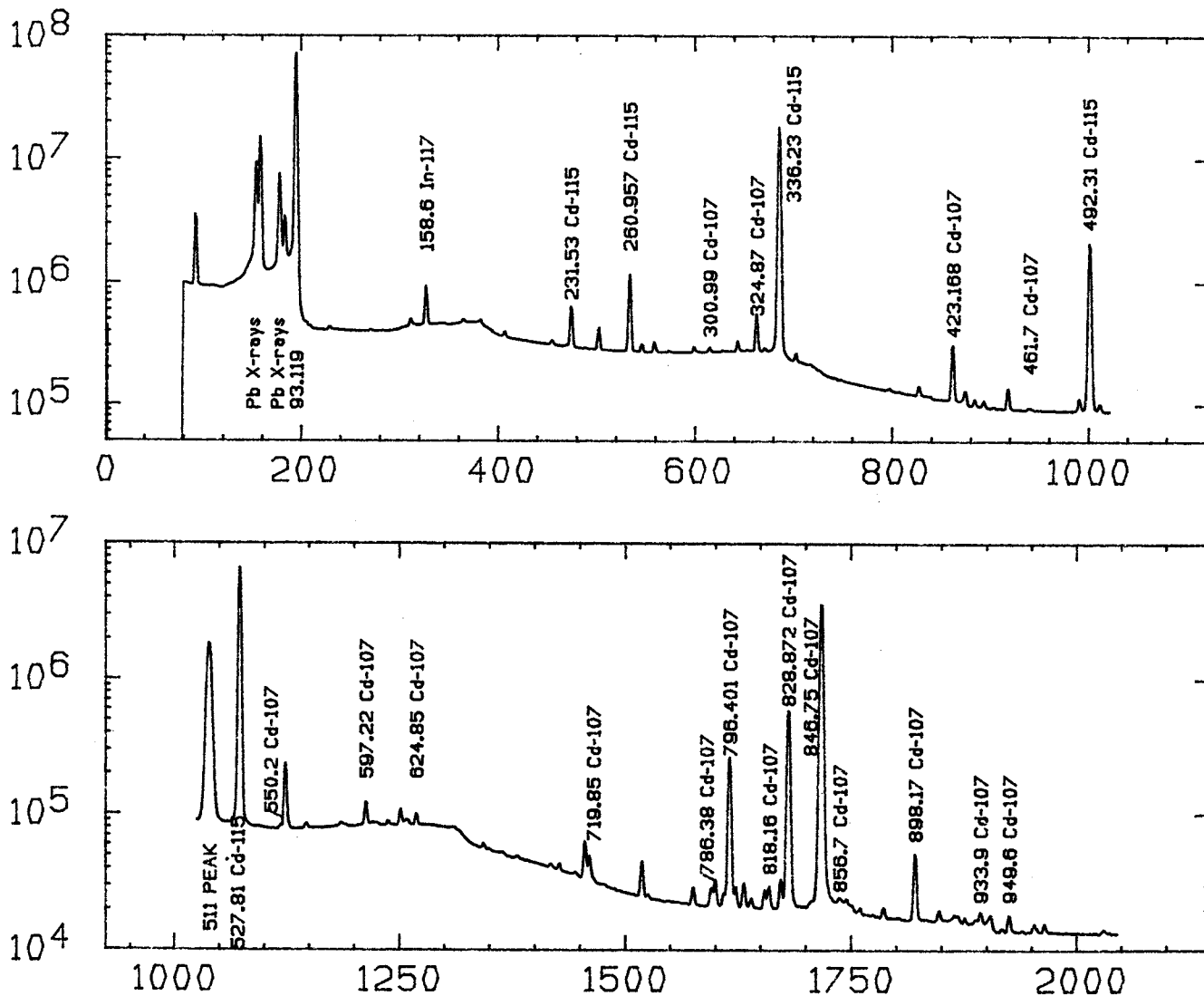


Fig. 2. Preliminary level scheme of ^{107}Ag .

W.A. Olivier, W.-T. Chou, R. Aryaeinejad, and Wm.C. McHarris

The study of odd-odd neutron deficient Re nuclei has continued at NSCL with a γ - γ coincidence study of ^{176}Re .¹

Interest in odd-odd Re nuclei has increased in the last five years. Three groups have been actively studying the odd-odd nuclei in the $^{176}\text{Re} - ^{182}\text{Re}$ region using in beam γ -ray spectroscopy.²⁻⁴ At one time the spectra produced by these reactions were thought to be too complex to analyze but it has been observed that heavy ion reactions populate only a limited number of the available high spin states in the nuclei. Then the nuclei de-excite through γ -ray emission in "klokast" bands to the yrast band. While the results for some nuclei are still difficult to interpret they offer great hope for further study in the region.

The reaction we studied at NSCL was $^{159}\text{Tb}(^{22}\text{Ne}, 5n\gamma)^{176}\text{Re}$ at 108 MeV. This was a record low beam energy (MeV/nucleon) accelerated by the K500 at NSCL. The target was a self-supporting 1.0 mg/cm^2 foil and γ -rays were detected with two 15% efficient bare Ge detectors positioned 5 cm. from the target. This is the highest mass projectile used to produce any of the odd-odd Re nuclei studied in-beam and promises to yield the highest observed angular momentum in these systems.

It has been observed that in even-even nuclei, a shape transition from a prolate core to an oblate core occurs at high spin for nuclei around this region. This is the result of nucleons of the core breaking the alignment with the core to form an oblate "girdle", and eventually an oblate core, which can carry larger amounts of angular momentum. Odd-odd nuclei have the advantage of already having the two odd particles positioned in this "girdle" which should lead to an easier shape transition than has been observed in the even-even nuclei.

In our recent experiment we observed γ -ray transitions in ^{176}Re . Although the analysis of the data is still in the preliminary stages we have identified two rotational bands in the nucleus. Very little was known about the structure of ^{176}Re prior to this work. There were two levels identified by the decay of ^{176}Os , a few low lying levels placed by coulomb excitation work, and one other in-beam study by Krejner, et. al. focusing on the doubly decoupled $1/2^-1/2^-$ band. We have observed the band to which they have assigned this structure.

The spectrum shown in Fig. 1 is a coincidence spectrum of the ^{176}Re . The large number of low energy γ -rays present indicate the presence of several rotational bands. At present we have only placed two of these low energy γ -rays in rotational bands, and have not observed any direct linking of these two bands.

One of the observed bands is built on the lowest observed transition at 170.3 keV. This band was observed by Krejner's group in Buenos Aires and determined to be the $1/2^-1/2^-$ band. The lowest observed level has a spin of 5^+ . The other band we have identified is built on a 183.9 keV transition. This band has not been reported in the literature. The spins of the levels in this band are uncertain at present although arguments can be made from the

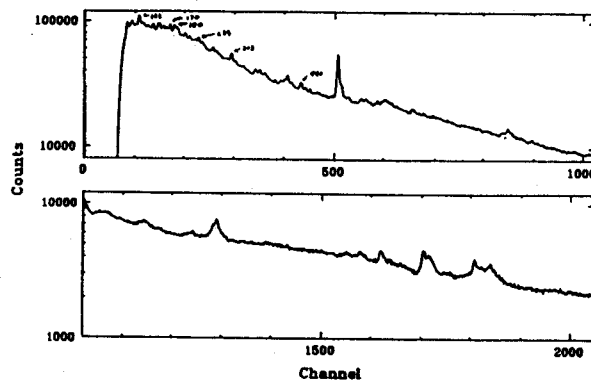


Fig. 1. A coincidence spectrum of ^{176}Re .

systematics of the region for an assignment of 7+.

References

Both bands feed a low-lying metastable state in the nucleus which de-excites by the emission of a 121.3 keV γ -ray. The half-life of the state was determined as shown in Fig. 2 to be approximately 48ns. This state then decays to the ground state in ^{176}Re .

A partial level scheme is shown in Fig. 3. We are confident that this will be greatly expanded as further analysis of the data is completed.

1. W.-T. Chou, W.A. Olivier, R. Aryaeinejad, and Wm.C. McHarris, Annual Report 1985, NSCL, Michigan State University, p.80 (1986)
2. M.F. Slaughter, R.A. Warner, T.L. Khoo, W.H. Kelly, and Wm.C. McHarris, Phys. Rev. C 29, 114 (1984).
3. Ts. Venkova, et. al., Annual Report 1985, IKP, KFA Julich, Jul-Spez-305 p.49 (1986)
4. J. Davidson, et. al., Z. Phys. A 324, 363 (1986)

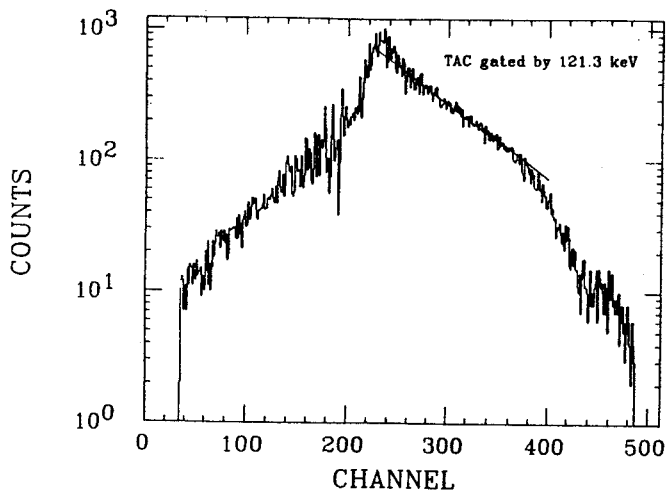


Fig. 2. Time spectrum gated by 121.3 keV peak

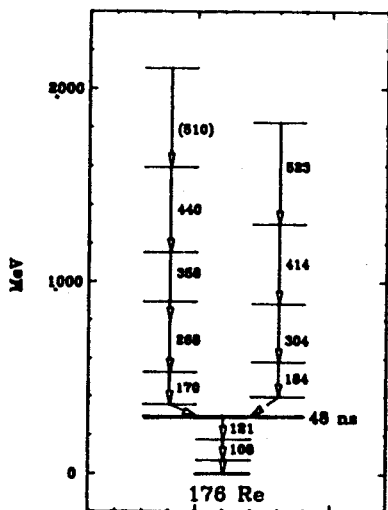


Fig. 3. Level scheme of ^{176}Re

A. Nadasen^a, F.D. Becchetti^a, J.W. Janecke^a, G. Gunderson^a, M. McMaster^a, A. Judd^a,
S. Villanneva^a, K.T. Hecht^a, J. Winfield, A. Galonsky and R.E. Warner^b

The cluster structure of ^{28}Si has been of interest to both theorists and experimentalists in recent years. Chung et al.¹ have predicted the existence of alpha-clusters in ^{28}Si and this has been experimentally verified by Carey et al.² and Anantaraman et al.³

Several other models of the structure of ^{28}Si have been developed by theorists. Most of them are built around a ^{16}O core. The $^{16}\text{O} + ^{12}\text{C}$ overlap in ^{28}Si has been given particular attention by Franey et al.,⁴ who predicted a 10% probability for this configuration. Hecht and Braunschweig⁵ also support his hypothesis, based on the prediction by Harvey et al.⁶ that the ground state of ^{28}Si may have a 20% probability of being prolate. The observation of these clusters in the electrofission of ^{28}Si ⁷ is the only experimental evidence thus far available.

In the light of the above predictions, we carried out an investigation of the existence of ^{12}C clusters in ^{28}Si by means of the quasi-free knockout reactions. We bombarded a ^{28}Si target with a 420 MeV ^{12}C beam from the K500 cyclotron at NSCL. The experiment was carried out in the 60" scattering chamber. Two $\Delta E - E$ Si telescopes were placed on opposite sides of the beam in a coplanar geometry to detect $^{12}\text{C} - ^{12}\text{C}$ coincidences. Measurements were made at angle pairs of $16^\circ / -69.6^\circ$, $24^\circ / -62.9^\circ$ and $32^\circ / -55.4^\circ$.

Identification of ^{12}C particles was performed in the forward angle detector telescope from $\Delta E - E$ measurements. True ^{12}C knockout events were identified through kinematic conditions between the two detector telescopes. Two-dimensional plots of the particle energy in one detector versus the energy in the other detector were obtained. Figure 1 shows a plot for the $16^\circ / -60.6^\circ$

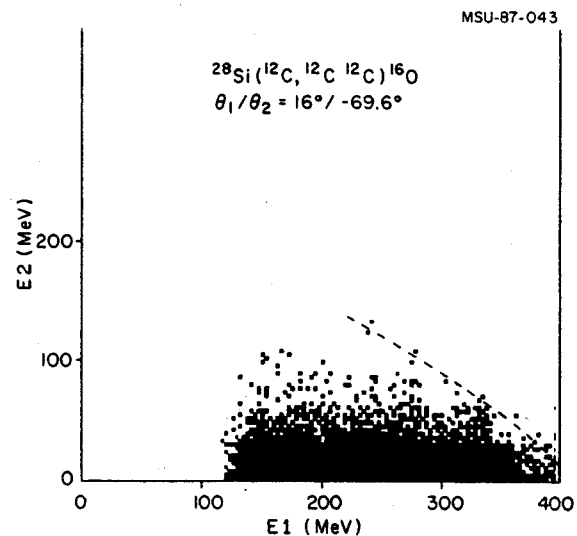


Fig. 1. Plot of E_1 vs. E_2 coincidence events with telescope 1 gated for ^{12}C . The dashed line represents the kinematic locus for quasi-free events.

measurement. The events for the quasi-free knockout reaction will lie along the kinematic locus (shown as a dashed line). The yields obtained for all three angle pairs indicate very small cross sections. The data seem to set an upper limit on the cluster probability which is significantly smaller than the theoretical predictions.

a. University of Michigan, Ann Arbor, MI.

References

1. W. Chung, J. van Hienen, B.H. Wildenthal and C.L. Bennett, *Phys. Lett.* **79B**, 381(1978).
2. T.a. Carey et al., *Phys. Rev. C* **29**, 1273(1984).
3. N. Anantaraman et al., *Phys. Rev. Lett.* **35**, 1131(1975).
4. M.A. Franey et al., *Phys. Lett.* **81B**, 132(1979).
5. K.T. Hecht and D. Braunschweig, *Phys. Rev.* **C17**, 396(1978); K.T. Hecht, private communication.
6. J.-P. Bernier and M. Harvey, *Nucl. Phys.* **A94**, 593(1967); J.P. Elliot and M. Harvey, *Proc. Roy. Soc.* **A272**, 557(1963)
7. A.M. Sandorfi et al., *Phys. Rev. Lett.* **38**, 1463(1977).

S. Fortier^a, S. Gales^a, S.M. Austin, W. Benenson, G.M. Crawley, C. Djalali, J. Winfield

Structures observed in heavy ion inelastic scattering spectra at high excitation energy in various systems have been interpreted in terms of multiphonon excitation of the target nuclei¹. In order to try to confirm the existence of these structures, which has been questioned recently² in the system $^{20}\text{Ne}+^{208}\text{Pb}$ at 30 MeV/A, and also to study any variation in the structure with incident energy, a high statistics experiment has been performed using a ^{20}Ne beam from the K500 cyclotron.

Inelastic scattering and one-nucleon-transfer reactions induced by ^{20}Ne on ^{90}Zr and ^{208}Pb have been studied at 500 and 600 MeV incident energies, using the S320 magnetic spectrograph. The high excitation energy parts of the four inelastic spectra accumulated at grazing angles are shown in figs. 1 and 2. In order to enhance the small oscillations present in the data, the spectra were smoothed using Fourier transformation techniques. They are displayed superimposed on the experimental points, given with their statistical error bars. The apparent excitation energies of the smoothed bumps in ^{208}Pb and ^{90}Zr can be compared with the average positions of the high-energy structures from ref. 1, observed in previous experiments involving several projectiles, and indicated above the spectra.

The $^{20}\text{Ne} + ^{208}\text{Pb}$ spectra are clearly dominated by two bumps, at 31 and 42.5 MeV for 30 MeV/A incident energy, and at 27.5 and 37 MeV for 25 MeV/A. This shift of the apparent excitation energies definitely excludes the possibility that these bumps originate from an excitation of the target nucleus. These kinematical characteristics are quite compatible with those expected for a transfer-evaporation process^{3,4}, where the ^{21}Ne ejectile strongly

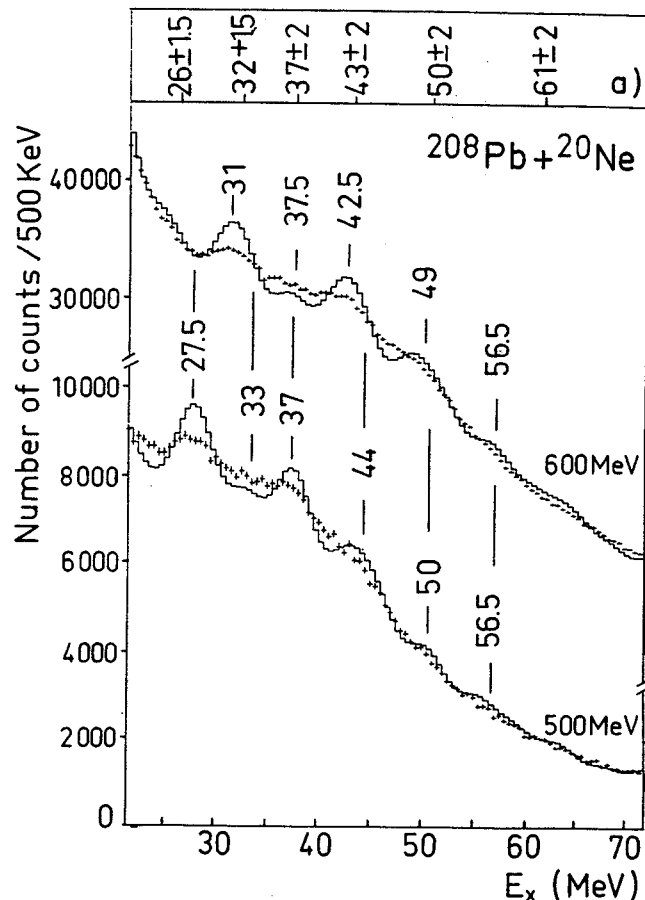


Fig. 1. High excitation energy part of the (Ne+Pb) inelastic scattering spectra to 30 MeV/A (above) and 25 MeV/A (below), at the grazing angle (respectively 9.5 and 11.5 dg (lab)). Experimental points are represented with their statistical error bars, together with the spectra smoothed by a Fourier transform analysis. At the top (a), the excitation energies from ref. 1) are given for comparison.

excited in a discrete unbound state would emit a neutron of about 300 keV, as already observed in a coincidence experiment³ involving the system $^{20}\text{Ne}+^{58}\text{Ni}$ at 11 MeV/A. The situation is not so clear for the $^{20}\text{Ne}+^{90}\text{Zr}$ system, where the transfer-evaporation bump exhibits a flat top with only very small oscillations, compatible with possible non-linearity defects in the detection system.

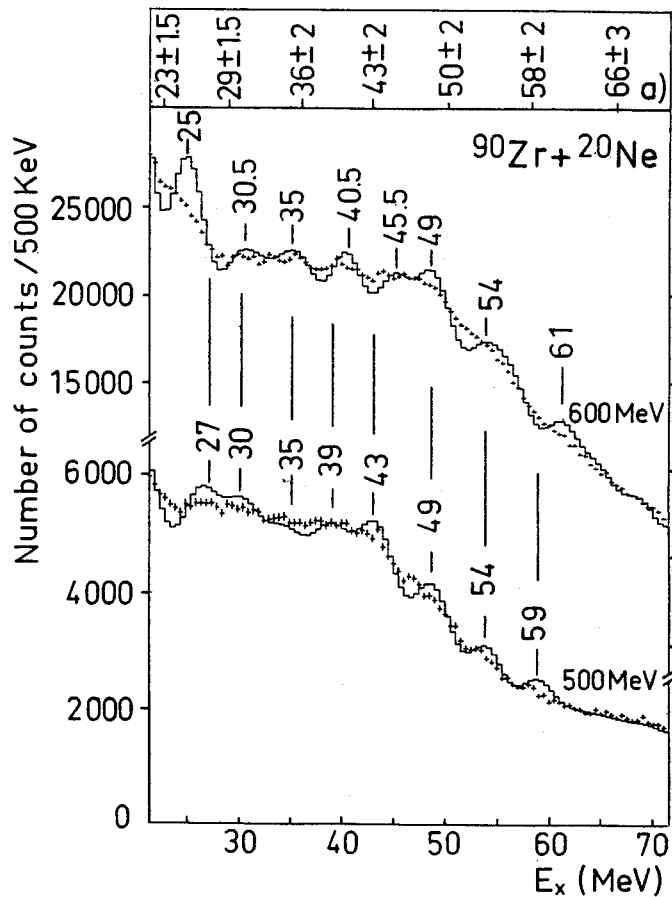


Fig. 2. Same as fig. 1 for the ($^{20}\text{Ne} + ^{208}\text{Pb}$) system. The detection angles are 5.3 dg and 6.4 dg (lab) at 30 and 25 MeV/A, respectively.

In conclusion, the high-excitation-energy resonances suggested in ref. 1 are not observed in the present experiment. Only an upper limit for the excitation cross-section of these states (about 1 mb/sr) could be determined from the present data.

a. IPN Orsay, France

References

1. N. Frascaria, Winter Meeting Nuclear Physics, Bormio (1986) and references therein. N. Frascaria et al., to be published.
2. M. Buenerd et al., Phys. Lett. 167B (1986) 379.
3. Y. Blumenfeld et al., Nucl. Phys. A445 (1985) 151.
4. H.G. Bohlen et al., Z. Phys A320 (1985) 237.